PALACKÝ UNIVERSITY OLOMOUC

FACULTY OF SCIENCE

Department of Optics

New methods for evaluating superpositions of highly squeezed states

BACHELOR'S THESIS

Vojtěch Kuchař

2024

UNIVERZITA PALACKÉHO V OLOMOUCI
PŘÍRODOVĚDECKÁ FAKULTA

Katedra optiky

Nové metody vyhodnocování kvality superpozic silně stlačených stavů

BAKALÁŘSKÁ PRÁCE

Vojtěch Kuchař

2024

PALACKÝ UNIVERSITY OLOMOUC

FACULTY OF SCIENCE

Department of Optics

New methods for evaluating superpositions of highly squeezed states

BACHELOR'S THESIS

Author: Vojtěch Kuchař

Study programme: B1701 Physics

Field of study: General Physics and Mathematical Physics

Form od study: Full-time

Supervisor: doc. Mgr. Petr Marek, Ph.D.

UNIVERZITA PALACKÉHO V OLOMOUCI

PŘÍRODOVĚDECKÁ FAKULTA

Katedra optiky

Nové metody vyhodnocování kvality superpozic silně stlačených stavů

BAKALÁŘSKÁ PRÁCE

Vypracoval:	Vojtěch Kuchař
Studijní program:	B1701 Fyzika
Studijní obor:	Obecná fyzika a matematická fyzika
Forma studia:	prezenční
Vedoucí práce:	doc. Mgr. Petr Marek, Ph.D.

Abstract

Eigenkets of electromagnetic field mode quadrature operators are unphysical states, which play an important part in bosonic implementations of quantum computers and in other areas of quantum optics. Their experimental preparation is inherently impossible, but they can be approximated using highly squeezed states and evaluated by means of quadrature squeezing. Superpositions of highly squeezed states, on the other hand, currently do not have any straightforward methods of evaluating how well they approximate superpositions of quadrature eigenkets. The construction of suitable evaluation methods for even superpositions of squeezed states is the main focus of this work.

Keywords

quantum optics, squeezed states, quantum superposition, continuous variables, quantum entanglement, quantum measurement, quantum metrology, number states, Fock basis, numerical optimization, beam splitter, quantum nondemolition measurement, cat states

Abstrakt

Vlastní vektory kvadraturních operátorů módu elektromagnetického pole jsou nefyzikální stavy, které hrají důležitou roli při návrhu bosonových kvantových počítačů a v jiných oblastech kvantové optiky. Připravit tyto stavy experimentálně není možné, lze je však aproximovat pomocí silně stlačených stavů a vyhodnotit prostřednictvím stlačení v dané kvadratuře. Pro superpozice stlačených stavů naopak v současné době neexistují žádné jednoduché metody vyhodnocení jejich kvality jakožto aproximace superpozic vlastních vektorů kvadraturního operátoru. Návrh vhodných metod vyhodnocování sudých superpozic stlačených stavů je hlavním zaměřením této práce.

Klíčová slova

kvantová optika, stlačené stavy, kvantová superpozice, spojité proměnné, kvantové provázání, kvantové měření, kvantová metrologie, Fokova báze, Fokův prostor, Fokovy stavy, numerická optimalizace, dělič svazku, kvantová nedemoliční interakce, stavy koček

Acknowledgements

First and foremost, I would like to thank my supervisor, Petr Marek, for his time and support, which made the thesis writing experience way more enjoyable than I expected it to be. I am also grateful to all those who taught me physics in the past, shaping my understanding and passion for the subject. My deepest appreciation goes to my friends, my girlfriend, and my family for helping me travel each and every path I chose in life.

Declaration

I hereby declare that I am the sole author of the presented thesis and that no sources, other than those listed in the bibliography and methods sections, have been used. I declare to have acknowledged the contributions of others through citations and that any sections lacking references are my own, developed independently under the guidance of my supervisor.

Declared in Olomouc on 16. 4. 2024 .....

Contents

List of Figures

Introduction

One of the main avenues in the ever-evolving landscape of quantum information, communication, and optics is the construction of fault-tolerant quantum computers utilizing continuous variables. More conventional approaches to quantum computing employ discrete two-level quantum systems – qubits, which can be physically implemented using superconducting circuits, quantum dots, and various other methods. Significant challenges emerge when implementing quantum error correction in this approach, as even the simplest error-correcting codes for two-level systems require deep redundancy and pose significant practical challenges. [1, 2, 3]

An alternative to this is to encode logical qubits into continuous variables, usually those associated with non-commuting quadrature operators of field modes, as exotic continuous variable states allow for sufficient correction of certain errors connected with their symmetries. This strategy comes with the benefit of potentially employing already existing optical communication infrastructure, but is equally applicable to superconducting microwave cavities and other systems, where quadrature operators are defined. Many proposed continuous variable quantum codes with error-correcting capabilities exist; nevertheless, one common thread tying many of them together is the need for quadrature eigenstates and their superpositions. [2, 4, 5, 6]

Quadrature eigenkets are intrinsically unphysical, contain an infinite amount of energy, and cannot be prepared experimentally. They need to be approximated for all practical applications, with one of their available approximations being squeezed states. The preparation of squeezed states and their superpositions is an active area of research and the degree to which simple squeezed states approximate quadrature eigenkets can be evaluated by quadrature squeezing; however, no straightforward methods for evaluating the degree to which superpositions of squeezed states approximate superpositions of quadrature eigenstates exist. [6, 7, 8, 9]

In this work, we investigate the properties of superpositions of displaced squeezed states, frequently referred to as squeezed cat states, and propose multiple methods for evaluating how well they approximate superpositions of quadrature eigenstates. We will employ analytical and numerical methods to compare the proposed metrics and discuss potential issues and outliers. The goal of this thesis is to find new methods for evaluating superpositions of highly squeezed states, which could potentially be used in their preparation and help pave the way to fault-tolerant quantum computation and communication.

Chapter I

Foundations

In the first chapter, we shall construct a basic theoretical framework, where squeezed states function as an approximation of quadrature eigenkets, and proceed to show why quantum state fidelity is not a good way to evaluate the suitability of such approximations. We will then explain the significance of quadrature eigenkets in the context of superposition states.

1.1 Quadrature eigenkets

Let us begin by considering an electromagnetic field mode described by the bosonic annihilation operator $\hat{a}$, which obeys the commutation relation

$$\left[\hat{a}, \hat{a}^\dagger\right] = 1, \tag{1.1.1}$$

where we have chosen natural units with $\hbar = 1$. We define quadrature operators $\hat{x}$ and $\hat{p}$ as [10]

$$\hat{x} = \frac{1}{\sqrt{2}}\left(\hat{a}^\dagger + \hat{a}\right), \tag{1.1.2}$$

$$\hat{p} = \frac{i}{\sqrt{2}}\left(\hat{a}^\dagger - \hat{a}\right). \tag{1.1.3}$$

It immediately follows from (1.1.1) that

$$[\hat{x}, \hat{p}] = i, \tag{1.1.4}$$

which is the canonical commutation relation. The spectra of both of these operators are unbounded and continuous, similarly to position and momentum [10]. We are particularly interested in quadrature eigenkets, which will be denoted by their corresponding eigenvalues, such as

$$\hat{x}\left|x_0\right\rangle = x_0\left|x_0\right\rangle, \tag{1.1.5}$$

where x_0 is an arbitrary eigenvalue of $\hat{x}$. We shall use $|x = x_0\rangle$ to refer to the same ket in cases where confusion with other bases could occur. It is apparent from (1.1.4) that the quadratures are incompatible observables and are thus bound by the uncertainty relation [11]

$$\operatorname{var}\hat{x} \cdot \operatorname{var}\hat{p} \geq \frac{1}{4}, \tag{1.1.6}$$

where the variance of an observable is defined as

$$\operatorname{var}\hat{A} = \left\langle \left(\hat{A} - \left\langle \hat{A} \right\rangle\right)^2 \right\rangle. \tag{1.1.7}$$

Note that for the $\hat{x}$ eigenket defined in equation (1.1.5), $\operatorname{var}\hat{x}$ will be zero, which means that $\operatorname{var}\hat{p}$ must diverge according to (1.1.6).

Quadrature variance divergence implies the divergence of energy for these states and quadrature eigenkets are thus unphysical and non-normalizable. This poses some interesting problems for the foundations of quantum mechanics and, for example, necessitates the mathematical construction of rigged Hilbert spaces [12]. In the following work, however, we shall focus on how these eigenkets can be approximated using physical states with the same expectation value and minimized quadrature variance.

1.2 Squeezed vacua

Let us start with the eigenket $|x = 0\rangle$. Its wave function in the $x-$representation can be regarded as the Dirac delta distribution, and a suitable approximation for this eigenket is the squeezed vacuum state. We define the vacuum state $|0\rangle$ by [13]

$$\hat{a}\,|0\rangle = 0 \tag{1.2.1}$$

and the squeezing operator $\hat{S}(\tilde{r})$ as

$$\hat{S}(\tilde{r}) \equiv \exp\left[\frac{1}{2}\left(\tilde{r}^*\hat{a}^2 - \tilde{r}\hat{a}^{\dagger 2}\right)\right], \tag{1.2.2}$$

where $\tilde{r} = re^{i\varphi}$ is the complex squeezing parameter. We will mostly work with the simplified form

$$\hat{S}(r) = \exp\left[\frac{r}{2}\left(\hat{a}^2 - \hat{a}^{\dagger 2}\right)\right], \tag{1.2.3}$$

where the squeezing parameter is set to be a real number. This simplification only allows squeezing in directions orthogonal to quadratures in the phase space, which is sufficient for our needs. The squeezed vacuum state is then

$$|\mathrm{SV}(r)\rangle = \hat{S}(r)\,|0\rangle. \tag{1.2.4}$$

The $x-$representation wave function of the vacuum is [10]

$$\langle x|0\rangle = \frac{1}{\sqrt[4]{\pi}} \exp\left(-\frac{x^2}{2}\right), \tag{1.2.5}$$

from which we can derive the squeezed vacuum wave function to be [14]

$$\langle x|\mathrm{SV}(r)\rangle = \frac{e^{r/2}}{\sqrt[4]{\pi}} \exp\left(-e^{2r}\frac{x^2}{2}\right). \tag{1.2.6}$$

The expectation value $\langle \mathrm{SV}(r)|\hat{x}|\mathrm{SV}(r)\rangle$ is zero per the symmetric wave function, we can thus determine the $\hat{x}$ variance of the squeezed vacuum state as

$$\mathrm{var}\,\hat{x} = \langle \mathrm{SV}(r)|\hat{x}^2|\mathrm{SV}(r)\rangle = \int_{-\infty}^{+\infty} \mathrm{d}x \,\langle \mathrm{SV}\,(r)|x\rangle\, x^2\, \langle x|\mathrm{SV}(r)\rangle = \int_{-\infty}^{+\infty} \frac{x^2 e^r}{\sqrt{\pi}} \exp\left(-x^2 e^{2r}\right) \mathrm{d}x, \tag{1.2.7}$$

which evaluates to

$$\mathrm{var}\,\hat{x} = \frac{1}{2e^{2r}}. \tag{1.2.8}$$

It is well known that squeezed vacua are minimum-uncertainty states [13, 14], which saturate the uncertainty relation (1.1.6), we can therefore also immediately write the $\hat{p}$ variance

$$\mathrm{var}\,\hat{p} = \frac{e^{2r}}{2}. \tag{1.2.9}$$

Given the expectation value of $\hat{x}$ and its variance for this state, we can conclude that in the limit of large squeezing as $r \to +\infty$, the squeezed vacuum state converges to the eigenket $|x = 0\rangle$, with its $\hat{p}$ variance diverging to infinity.

1.3 Fidelity and variance

Given the task of minimizing the quadrature variance of a squeezed vacuum state, two intuitive ways to do so are by measuring the variance, or by comparing the state to a different state, for which the variance is known. Let us now focus on the second method. This might seem unnecessary in the context of squeezed vacua, but it proves to be a useful discussion in preparation for larger problems ahead.

One way to measure the similarity of quantum states is the quantum state fidelity F. In the most general case, given two density operators $\hat{\rho}_1$ and $\hat{\rho}_2$ describing two quantum states, we define their fidelity as [15]

$$F\left(\hat{\rho}_1, \hat{\rho}_2\right) \equiv \left(\mathrm{tr}\sqrt{\sqrt{\hat{\rho}_1}\hat{\rho}_2\sqrt{\hat{\rho}_1}}\right)^2. \tag{1.3.1}$$

If we consider one of the states to be pure $\hat{\rho}_1 = |\psi_{\hat{\rho}_1}\rangle\langle\psi_{\hat{\rho}_1}|$, we can use $\hat{\rho}_1^2 = \hat{\rho}_1 \implies \sqrt{\hat{\rho}_1} = \hat{\rho}_1$ to rewrite (1.3.1) as

$$F\left(\hat{\rho}_1, \hat{\rho}_2\right) = \left(\mathrm{tr}\sqrt{|\psi_{\hat{\rho}_1}\rangle\langle\psi_{\hat{\rho}_1}|\,\hat{\rho}_2\,|\psi_{\hat{\rho}_1}\rangle\langle\psi_{\hat{\rho}_1}|}\right)^2, \tag{1.3.2}$$

where $\langle\psi_{\hat{\rho}_1}|\hat{\rho}_2|\psi_{\hat{\rho}_1}\rangle$ is a number and $\left(\mathrm{tr}\sqrt{|\psi_{\hat{\rho}_1}\rangle\langle\psi_{\hat{\rho}_1}|}\right)^2 = 1$, thus, the fidelity for a mixed state and a pure state is

$$F\left(\hat{\rho}_1, \hat{\rho}_2\right) = \langle\psi_{\hat{\rho}_1}|\hat{\rho}_2|\psi_{\hat{\rho}_1}\rangle\,, \tag{1.3.3}$$

from which we can determine the fidelity for two pure states as

$$F\left(\hat{\rho}_1, \hat{\rho}_2\right) = \left|\langle\psi_{\hat{\rho}_1}|\psi_{\hat{\rho}_2}\rangle\right|^2. \tag{1.3.4}$$

Equation (1.3.4) can be intuitively understood as the square of the overlap between the two states. It also implies that for any pure $\psi_{\hat{\rho}_1}, \psi_{\hat{\rho}_2}$ we have $0 \leq F\left(\hat{\rho}_1, \hat{\rho}_2\right) \leq 1$, $F\left(\hat{\rho}_1, \hat{\rho}_2\right) = 1 \iff \psi_{\hat{\rho}_1} = \psi_{\hat{\rho}_2}$ and $F\left(\hat{\rho}_1, \hat{\rho}_2\right) = F\left(\hat{\rho}_2, \hat{\rho}_1\right)$. It can be shown that these properties extend to the general case of mixed states as well [15].

Let us examine how the fidelity of two squeezed vacuum states relates to their $\hat{x}$ variance. Following equation (1.3.4), we can calculate the fidelity of two squeezed vacuum states with different squeezing parameters r_1, r_2 as

$$\begin{aligned} F\left(\hat{\rho}_{\mathrm{SV}(r_1)}, \hat{\rho}_{\mathrm{SV}(r_2)}\right) &= \left|\langle \mathrm{SV}\left(r_1\right)|\mathrm{SV}\left(r_2\right)\rangle\right|^2 = \left|\int_{-\infty}^{+\infty} \mathrm{d}x\, \langle \mathrm{SV}\left(r_1\right)|x\rangle\, \langle x|\mathrm{SV}\left(r_2\right)\rangle\right|^2 \\ &= \left|\int_{-\infty}^{+\infty} \frac{e^{(r_1+r_2)/2}}{\sqrt{\pi}} \exp\left[-\frac{x^2}{2}\left(e^{2r_1} + e^{2r_2}\right)\right] \mathrm{d}x\right|^2 = \frac{2e^{r_1+r_2}}{e^{2r_1} + e^{2r_2}}. \end{aligned} \tag{1.3.5}$$

In the rest of this section we shall denote $F\left(\hat{\rho}_{\mathrm{SV}(r_1)}, \hat{\rho}_{\mathrm{SV}(r_2)}\right)$ as F for simplicity. If we now consider F and r_1 to be known, we obtain two possible solutions for r_2 in the form

$$r_2 = r_1 + \ln\left(\frac{1 \pm \sqrt{1 - F^2}}{F}\right). \tag{1.3.6}$$

Equation (1.3.6) says that given a squeezed vacuum state with a squeezing parameter r_1, all squeezed vacuum states which achieve fidelity F or higher with the given state must satisfy $r_2 \in \left[r_1 + \ln\left(\frac{1-\sqrt{1-F^2}}{F}\right), r_1 + \ln\left(\frac{1+\sqrt{1-F^2}}{F}\right)\right]$, where $[,]$ is a closed interval. We can easily translate this into the language of $\hat{x}$ variances by comparing equations (1.3.6) and (1.2.8). It turns out to be useful to examine the ratio k between variances of $\hat{x}$ for the two squeezed vacua in question as a function of their fidelity:

$$k(F) = \frac{\langle \mathrm{SV}\left(r_1\right)|\hat{x}^2|\mathrm{SV}\left(r_1\right)\rangle}{\langle \mathrm{SV}\left(r_2\right)|\hat{x}^2|\mathrm{SV}\left(r_2\right)\rangle} = \frac{e^{2r_2}}{e^{2r_1}} = \frac{\exp\left(2r_1\right)\exp\left[2\ln\left(\frac{1\pm\sqrt{1-F^2}}{F}\right)\right]}{\exp\left(2r_1\right)} = \left(\frac{1 \pm \sqrt{1 - F^2}}{F}\right)^2. \tag{1.3.7}$$

The ratio of variances for two squeezed vacuum states with fidelity F or higher must thus fall into the interval $k(F) \in \left[\left(\frac{1-\sqrt{1-F^2}}{F}\right)^2, \left(\frac{1+\sqrt{1-F^2}}{F}\right)^2\right]$, regardless of their specific squeezing. The two values are reciprocal – when we find two squeezed vacua exactly satisfying the fidelity requirement, they form a unique minimum/maximum variance pair. The interval of possible variances can be plotted as a function of minimum fidelity, see figure 1.1.

It is apparent from figure 1.1 that in a logarithmic plot, the maximum and minimum variance ratios for a given fidelity form a symmetric area centered at $k = 1$, where $F = 1$ can only be achieved by states with the same variance and $F > 0$, on the other hand, is satisfied by any two finitely squeezed vacuum states. Both of these extremes are to be expected.

One thing to note, however, is that fidelity values, which we may consider quite high intuitively, do not actually imply much for the variance of a quantum state. It can be readily shown from (1.3.7) that for $F = 0.9$ there exist two squeezed vacuum states whose variances differ from each other by a factor of 2.55 and even for $F = 0.99$ this factor is still 1.33. This of course is just a question of how we view fidelity and what our expectations for the states are based on this number, but it does beg the question of whether there is any connection between the fidelity of two states and their quadrature variances in the most general case.

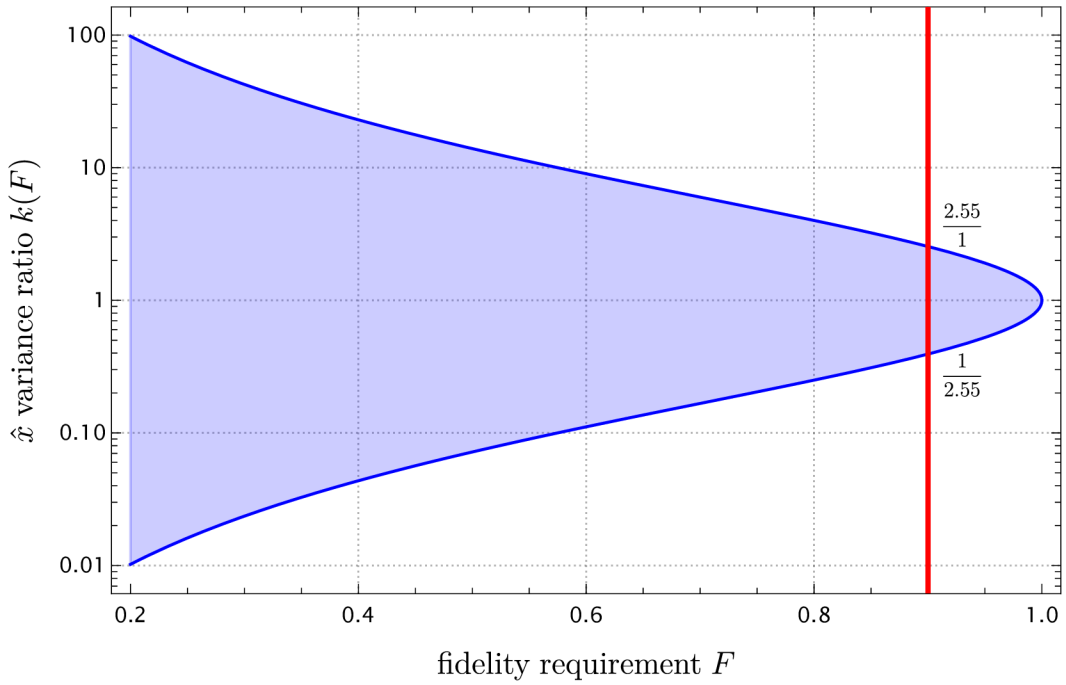

Figure 1.1: Logarithmic plot of all possible variance ratios for two squeezed vacuum states with a given minimum fidelity requirement. The blue lines represent extreme cases, which exactly satisfy the fidelity requirement, light blue filling signifies states with fidelity greater or equal to the requirement. Fidelity requirement of 0.9 is emphasized by a red line, with both the maximum and minimum ratios evaluated (these amount to fidelity values of exactly 0.9).

1.4 How fidelity fails us

It turns out, it can be proven that, given any pure state $\hat{\rho}_1$, there exists a state $\hat{\rho}_2$ such that $F(\hat{\rho}_1, \hat{\rho}_2) \geq F_0$ and $(\operatorname{var} \hat{x})_{\hat{\rho}_2} \geq K$, where $0 \leq F_0 < 1$ and $0 \leq K$ are arbitrary real numbers. This means that given any fidelity requirement F_0 and any pure state, we can construct a state satisfying this requirement with arbitrarily large $\hat{x}$ variance, the only exception being $F_0 = 1$.

In order to prove this, let us make a slight modification to equation (1.3.3) by rewriting the mixed state as a sum of projectors onto pure states

$$F(\hat{\rho}_1, \hat{\rho}_2) = \langle \psi_{\hat{\rho}_1} | \hat{\rho}_2 | \psi_{\hat{\rho}_1} \rangle = \langle \psi_{\hat{\rho}_1} | \sum_{i=1}^{n} p_i \, |\psi_i\rangle\langle\psi_i| | \psi_{\hat{\rho}_1} \rangle = \sum_{i=1}^{n} p_i \, |\langle \psi_i | \psi_{\hat{\rho}_1} \rangle|^2 . \tag{1.4.1}$$

We prove the existence of $\hat{\rho}_2$ by explicitly constructing it as

$$\hat{\rho}_2 = F_0 \, |\psi_{\hat{\rho}_1}\rangle\langle\psi_{\hat{\rho}_1}| + (1 - F_0) \, |\mathrm{SV}(r)\rangle\langle\mathrm{SV}(r)| , \tag{1.4.2}$$

where we have used the fact that $\hat{\rho}_1$ is pure and where the squeezing parameter r is to be determined later. Choosing probability coefficients in $\hat{\rho}_2$ in this way ensures the state is normalized. Equation (1.4.1) directly implies

$$F(\hat{\rho}_1, \hat{\rho}_2) = F_0 \, |\langle \psi_{\hat{\rho}_1} | \psi_{\hat{\rho}_1} \rangle|^2 + (1 - F_0) \, |\langle \mathrm{SV}(r) | \psi_{\hat{\rho}_1} \rangle|^2 , \tag{1.4.3}$$

where $|\langle \psi_{\hat{\rho}_1} | \psi_{\hat{\rho}_1} \rangle|^2 = 1, (1 - F_0) > 0$ and $|\langle \mathrm{SV}(r) | \psi_{\hat{\rho}_1} \rangle|^2 \geq 0$, thus $F(\hat{\rho}_1, \hat{\rho}_2) \geq F_0$ for any squeezing parameter r. The variance of $\hat{x}$ is just an expectation value per equation (1.1.7) and as such reduces to the weighted sum of expectation values for the constituent pure states

$$(\operatorname{var} \hat{x})_{\hat{\rho}_2} = F_0 \, (\operatorname{var} \hat{x})_{\hat{\rho}_1} + (1 - F_0) \, (\operatorname{var} \hat{x})_{\mathrm{SV}(r)} , \tag{1.4.4}$$

where we can use (1.2.8) and $(\operatorname{var} \hat{x})_{\hat{\rho}_2} \geq K$ to obtain

$$r \leq \ln \sqrt{\frac{1 - F_0}{2 \left[K - F_0 \, (\operatorname{var} \hat{x})_{\hat{\rho}_1} \right]}}, \tag{1.4.5}$$

which proves the existence of $\hat{\rho}_2$ for $K > F_0 \, (\operatorname{var} \hat{x})_{\hat{\rho}_1}$. This is sufficient, as not satisfying this condition implies $\hat{\rho}_1$ itself has an $\hat{x}$ variance larger than K and therefore $\hat{\rho}_2 = \hat{\rho}_1$ is the trivial solution in such case.

We have thus proven that even two states with arbitrarily large non-unitary fidelity can have arbitrarily different quadrature variances, which means that if we want to capture the variance of states into some kind of metric, an important task in approximating quadrature eigenkets, it seems necessary to look elsewhere.

1.5 Significance of quadrature eigenkets

We have not yet fully explained the uses of quadrature eigenkets and their approximations and a good time to do so would be now, before diving into any larger problems. Squeezed vacuum states themselves are often used not only while preparing some of the states mentioned later [8], but also in the quest to reduce quantum noise in complex optical experiments, such as the LIGO Collaboration [16]. Things become even more interesting once we consider superpositions of two or more quadrature eigenkets.

1.5.1 Squeezed cat states

One of the simplest superpositions to consider is the even eigenket superposition

$$|C_{\alpha,\infty}\rangle \equiv |\alpha\rangle + |-\alpha\rangle\,. \tag{1.5.1}$$

Following an argument similar to that in section 1.2, we can argue that this state can be approximated by the state

$$|C_{\alpha,r}\rangle \equiv \frac{1}{N_{\alpha,r}}\Big(|\alpha,r\rangle + |-\alpha,r\rangle\Big), \tag{1.5.2}$$

where $N_{\alpha,r}$ is a normalization constant and $|\alpha,r\rangle$ is the squeezed-displaced state

$$|\alpha,r\rangle = \hat{D}_x(\alpha)\hat{S}(r)\,|0\rangle \tag{1.5.3}$$

defined using the x displacement operator [10]

$$\hat{D}_x(\alpha) \equiv \exp\left[\frac{\alpha}{\sqrt{2}}\left(\hat{a}^\dagger - \hat{a}\right)\right] = \exp\left(-i\alpha\hat{p}\right). \tag{1.5.4}$$

The state (1.5.2) is a special case of a more general state

$$|C_{\tilde{\alpha},\tilde{r}}\rangle = \frac{1}{N_{\tilde{\alpha},\tilde{r}}}\Big(|\tilde{\alpha},\tilde{r}\rangle + |-\tilde{\alpha},\tilde{r}\rangle\Big), \tag{1.5.5}$$

where $\tilde{\alpha},\tilde{r}$ are complex numbers and where general complex forms of the displacement and squeezing operator are used. States of the form (1.5.5) are sometimes called squeezed cat states [4], as opposed to the case of $\tilde{r}=0$, i.e. the superposition of coherent states, which is often called the cat state [17]. Cat states themselves can be used to develop quantum computational schemes [18, 19] and can be prepared by means of photon subtraction [20], however, squeezed cat states offer some further possibilities.

We will examine the properties of squeezed cat states later, but for now, we can note that, in the limit of large squeezing, squeezed cat states are invariant under certain translations, which allows us to perform approximate error correction in quantum codes based upon them [4]. Squeezed cat states can also be used to prepare GKP states [5, 7, 9], which makes them invaluable for many proposed bosonic quantum codes.

1.5.2 GKP states

Some more complicated cases of quadrature eigenket superpositions were introduced in [6] and are now usually called GKP states after the authors. We have already mentioned that certain schemes for their preparation include the use of squeezed cat states, but let us also briefly introduce the states themselves and their use. The two GKP states can be defined as [21]

$$|j_{\mathrm{GKP}}\rangle \equiv \left(2\sqrt{\pi}\right)^{1/2} \sum_{n=-\infty}^{+\infty} |x = (2n + j)\sqrt{\pi}\rangle \tag{1.5.6}$$

for $j = 0, 1$. GKP states find their use in quantum computing because they form a periodic lattice in the phase space, which allows for very effective correction of errors that exhibit as a displacement smaller than the lattice period in the GKP code [6]. These errors are associated with photon loss [2], and as such it is impossible to avoid them and quite useful to be able to correct them. Needless to mention, GKP states again have to be physically approximated by superpositions of squeezed states [6, 21] as they comprise of quadrature eigenkets, which we have established to be unphysical. Although the GKP code was very much ahead of its time, it is not perfect and we can see see that it is for example not robust against dephasing errors, as GKP states do not possess the rotational symmetries that states in some other proposed bosonic codes do [2].

In recent years, the formalism of squeezed states has also spread from quantum optics into theoretical quantum descriptions of seemingly unrelated phenomena, such as black hole evaporation [22], antiferromagnetism [23] and even into descriptions of quantum gravity and its potential detection [24], so there seems to be enough incentive to study them further.

Chapter II

Squeezed cat states

In the following chapters, we will turn our attention to how the quality of squeezed cat states can be evaluated. We choose to focus on these states, as the discussion in section 1.5 shows that they can be used either to create quantum computing codes based directly upon them or as resources to prepare more complex and possibly even more useful quantum states. Let us start by examining them more thoroughly.

2.1 Representations and visualization

For the purposes of this thesis, the squeezed cat state is to be understood as the even superposition of squeezed-displaced states with real displacement and real squeezing as defined in equation (1.5.2). Rewriting the squeezed displaced states using equation (1.5.3) we obtain

$$|C_{\alpha,r}\rangle = \frac{1}{\sqrt{2\left[1+\exp\left(-\alpha^2 e^{2r}\right)\right]}}\left(\hat{D}_x(\alpha)\hat{S}(r)\,|0\rangle + \hat{D}_x(-\alpha)\hat{S}(r)\,|0\rangle\right), \tag{2.1.1}$$

where we can use the wave function of the squeezed vacuum state (1.2.6) to determine

$$\langle x|C_{\alpha,r}\rangle = \frac{1}{N'_{\alpha,r}}\left[\exp\left(-e^{2r}\frac{(x-\alpha)^2}{2}\right) + \exp\left(-e^{2r}\frac{(x+\alpha)^2}{2}\right)\right], \tag{2.1.2}$$

the normalization constant is

$$N'_{\alpha,r} = \exp\left(\frac{-\alpha^2 e^{2r} - r}{2}\right)\sqrt{2\sqrt{\pi}\left[1+\exp\left(\alpha^2 e^{2r}\right)\right]}. \tag{2.1.3}$$

Note that the probability distribution of x for a squeezed cat state

$$P_{\mathrm{cat}_{\alpha,r}}(x) = |\langle x|C_{\alpha,r}\rangle|^2 = \frac{1}{{N'_{\alpha,r}}^2}\left[\exp\left(-e^{2r}\frac{(x-\alpha)^2}{2}\right) + \exp\left(-e^{2r}\frac{(x+\alpha)^2}{2}\right)\right]^2 \tag{2.1.4}$$

is quite similar to

$$P_{\mathrm{mix}_{\alpha,r}}(x) = \langle x|\rho_{\mathrm{mix}_{\alpha,r}}|x\rangle = \frac{e^r}{2\sqrt{\pi}}\left[\exp\left[-e^{2r}\left(x-\alpha\right)^2\right] + \exp\left[-e^{2r}\left(x+\alpha\right)^2\right]\right], \tag{2.1.5}$$

which is the probability distribution of x for a mixture of two squeezed-displaced states

$$\hat{\rho}_{\mathrm{mix}_{\alpha,r}} = \frac{1}{2}\Big(|\alpha,r\rangle\langle\alpha,r| + |-\alpha,r\rangle\langle-\alpha,r|\Big), \tag{2.1.6}$$

the only difference between (2.1.4) and (2.1.5) being the cross term and normalization. This is clearly visible when we construct the density matrix for the squeezed cat state

$$\hat{\rho}_{\mathrm{cat}_{\alpha,r}} = \frac{1}{2\left[1+\exp\left(-\alpha^2 e^{2r}\right)\right]}\Big(|\alpha,r\rangle\langle\alpha,r| + |-\alpha,r\rangle\langle-\alpha,r| + |\alpha,r\rangle\langle-\alpha,r| + |-\alpha,r\rangle\langle\alpha,r|\Big). \tag{2.1.7}$$

We can quantify their similarity by integrating the squared difference between the probability distributions over all quadrature eigenvalues

$$\Delta^2 P(\alpha,r) = \int_{-\infty}^{+\infty} \mathrm{d}x\, \left[P_{\mathrm{cat}_{\alpha,r}}(x) - P_{\mathrm{mix}_{\alpha,r}}(x)\right]^2. \tag{2.1.8}$$

This is simply the squared L_2-metric-induced distance between the two functions, which is equal to zero for probability distributions equal almost everywhere [25]. It is apparent from the plots in figure 2.1 that $\Delta^2 P(\alpha,r)$ is approximately equal to zero for sufficiently separated superpositions (α and r large), which indicates that the probability distributions are extremely similar that case. We can see that the probability distributions are also identical for the case of $\alpha = 0$, which is to be expected, as in that case, both of these states just turn into squeezed vacua.

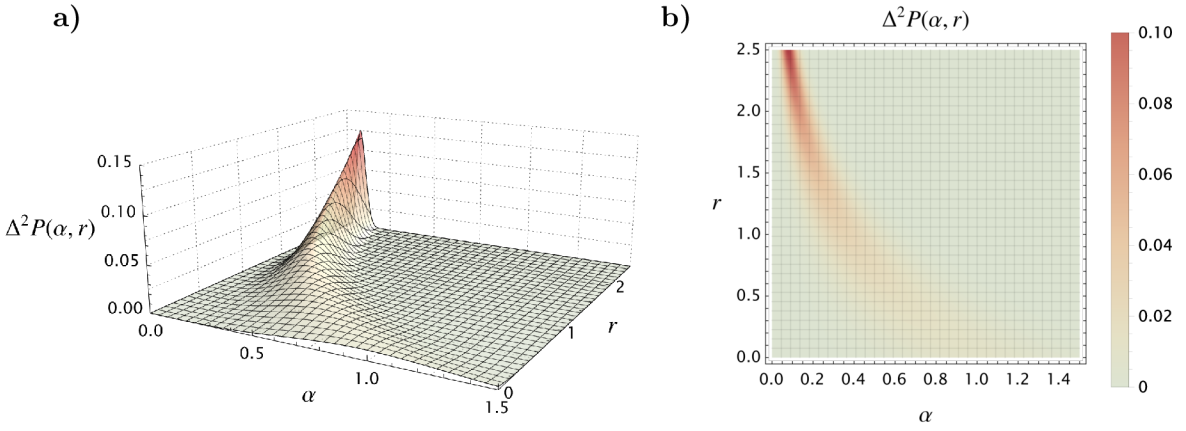

Figure 2.1: **a)** 3D plot and **b)** density plot of $\Delta^2 P(\alpha,r)$ as a function of α and r. For sufficiently squeezed and sufficiently displaced states, the probability distributions of $\hat{x}$ for the squeezed cat state (2.1.7) and the mixed state (2.1.6) are practically identical.

It is therefore impossible to fully characterize the squeezed cat state $\hat{\rho}_{\mathrm{cat}_{a,r}}$ simply by examining it in the $x-$representation, even though that seemed sufficient for one squeezed state. In order to fully understand superpositions of this sort, we will have to resort other representations.

To find the $p-$representation of a squeezed cat state, we insert the completeness relation [11]

$$\begin{aligned}\langle p|C_{\alpha,r}\rangle &= \int_{-\infty}^{+\infty} \mathrm{d}x\, \langle p|x\rangle\, \langle x|C_{\alpha,r}\rangle \\ &= \int_{-\infty}^{+\infty} \frac{\exp\left(-ipx\right)}{N'_{\alpha,r}\sqrt{2\pi}} \left[\exp\left(-e^{2r}\frac{(x-\alpha)^2}{2}\right) + \exp\left(-e^{2r}\frac{(x+\alpha)^2}{2}\right)\right] \mathrm{d}x \end{aligned} \tag{2.1.9}$$

and perform the resultant Fourier transform to obtain

$$\langle p|C_{\alpha,r}\rangle = \frac{2}{e^r N'_{\alpha,r}} \exp\left(-e^{-2r}\frac{p^2}{2}\right) \cos\left(\alpha p\right). \tag{2.1.10}$$

The process for mixed states is quite similar, even though it is necessary to insert the completeness relation twice in order to transform all matrix elements

$$\begin{aligned}\langle p_1|\hat{\rho}_{\mathrm{mix}_{\alpha,r}}|p_2\rangle &= \iint_{-\infty}^{+\infty} \mathrm{d}x_1\mathrm{d}x_2\, \langle p_1|x_1\rangle\, \langle x_1|\hat{\rho}_{\mathrm{mix}_{\alpha,r}}|x_2\rangle\, \langle x_2|p_2\rangle \\ &= \iint_{-\infty}^{+\infty} \frac{e^r \exp\left(-ip_1x_1\right)\exp\left(ip_2x_2\right)}{4\sqrt{\pi}^3} \left\{\exp\left[-e^{2r}\left[\frac{(x_1-\alpha)^2}{2} + \frac{(x_2-\alpha)^2}{2}\right]\right]\right. \\ &\quad \left. + \exp\left[-e^{2r}\left[\frac{(x_1+\alpha)^2}{2} + \frac{(x_2+\alpha)^2}{2}\right]\right]\right\} \mathrm{d}x_1\mathrm{d}x_2, \end{aligned} \tag{2.1.11}$$

from which we obtain

$$\langle p_1|\hat{\rho}_{\mathrm{mix}_{\alpha,r}}|p_2\rangle = \frac{1}{e^r\sqrt{\pi}} \exp\left[-e^{-2r}\left(\frac{p_1^2}{2} + \frac{p_2^2}{2}\right)\right] \cos\left[\alpha\left(p_2 - p_1\right)\right]. \tag{2.1.12}$$

The probability distribution for the squeezed cat state being

$$\left|\langle p|C_{\alpha,r}\rangle\right|^2 = \frac{4}{e^{2r}{N'_{\alpha,r}}^2} \exp\left(-e^{-2r}p^2\right) \cos^2\left(\alpha p\right), \tag{2.1.13}$$

as opposed to the probability distribution for the mixed state

$$\langle p|\hat{\rho}_{\mathrm{mix}_{\alpha,r}}|p\rangle = \frac{1}{e^r\sqrt{\pi}} \exp\left(-e^{-2r}p^2\right). \tag{2.1.14}$$

We can see that in the $p-$representation, the mixed state behaves like a squeezed vacuum state, whereas the squeezed cat state contains the cosine term, which implies that some eigenvalues of $\hat{p}$ are not allowed at all. It also implies periodicity and translational invariance with a period of $\Delta p = \frac{2k\pi}{\alpha}, k \in \mathbb{Z}$ in the limit as $r \to +\infty$, whereas the mixture (2.1.14) is invariant under any p translation in the same limit. These properties can be attributed to the cross terms in (2.1.7) and distinguish the superposition state from the mixture.

2.1.1 Phase space formalism

An even more suggestive way to study quantum states is with the help of quasi-probability distributions, arguably the most famous one being the Wigner quasi-probability distribution [10], also sometimes called the Wigner function. We define it for a quantum state described by the density operator $\hat{\rho}$ as

$$W(x,p) \equiv \frac{1}{2\pi}\int_{-\infty}^{+\infty} \exp(ipt)\ \langle x - t/2|\hat{\rho}|x + t/2\rangle\, \mathrm{d}t. \tag{2.1.15}$$

It essentially acts as a joint probability distribution for x and p, and we can obtain their respective distributions simply by integrating over the other variable. This highlights the importance of Wigner distributions for visualization, as they combine probability distributions for both quadratures. In order to achieve a full formulation of quantum mechanics in the phase space, we also need a mapping between operators in the Hilbert space and the phase space, which we usually call the Weyl transform [26]. This transformation is defined similarly to the Wigner function itself

$$\tilde{A}(x,p) \equiv \int_{-\infty}^{+\infty} \exp(ipt)\ \langle x - t/2|\hat{A}|x + t/2\rangle\, \mathrm{d}t, \tag{2.1.16}$$

where $\tilde{A}$ is the transformed operator in the phase space. The phase space formalism allows us to calculate expectation values of operators only using the Wigner function of the quantum state and the Weyl transform of the operator [10]

$$\left\langle \hat{A} \right\rangle = \iint_{-\infty}^{+\infty} W(x,p)\, \tilde{A}(x,p)\ \mathrm{d}x\, \mathrm{d}p. \tag{2.1.17}$$

We can calculate the Wigner function for the squeezed cat state as

$$\begin{aligned} W_{\mathrm{cat}}(x,p) &= \frac{1}{2\pi}\int_{-\infty}^{+\infty} \exp(ipt)\, \langle x - t/2|C_{\alpha,r}\rangle\langle C_{\alpha,r}|x + t/2\rangle\, \mathrm{d}t \\ &= \frac{2\cos(2\alpha p)\exp\left[e^{2r}\left(2\alpha x + \alpha^2\right)\right] + \exp\left(4\alpha e^{2r}x\right) + 1}{2\pi\left[\exp\left(\alpha^2 e^{2r}\right) + 1\right]} \\ &\quad \times \exp\left[e^{2r}\left(-x^2 - 2\alpha x\right) - p^2 e^{-2r}\right], \end{aligned} \tag{2.1.18}$$

whereas for the mixed state, we obtain

$$\begin{aligned} W_{\mathrm{mix}}(x,p) &= \frac{1}{4\pi}\int_{-\infty}^{+\infty} \exp(ipt)\, \langle x - t/2|\left(|\alpha,r\rangle\langle\alpha,r| + |-\alpha,r\rangle\langle -\alpha,r|\right)|x + t/2\rangle\, \mathrm{d}t \\ &= \frac{\exp\left(4\alpha e^{2r}x\right) + 1}{2\pi}\exp\left[e^{2r}\left(-x^2 - 2\alpha x - \alpha^2\right) - p^2 e^{-2r}\right]. \end{aligned} \tag{2.1.19}$$

Wigner functions for both states are plotted in figure 2.2, where, in the case of the squeezed cat state, we can observe negativity of the Wigner function, which is a characteristic of all non-Gaussian pure states [10]. It can also be seen why the states behave identically in the $x-$representation, as the interference fringes cancel out while integrating over p.

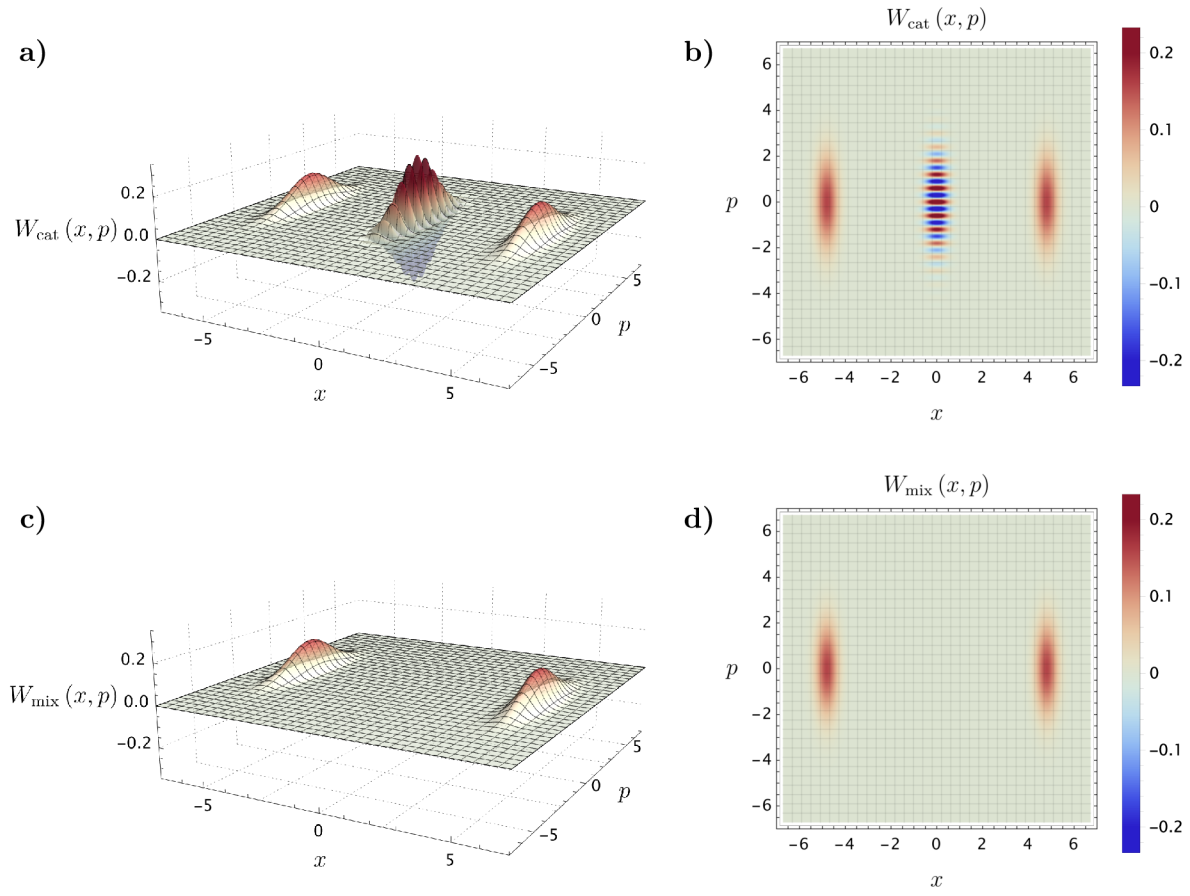

Figure 2.2: **a)** 3D plot and **b)** density plot of the Wigner function for the squeezed cat state, **c)** 3D plot and **d)** density plot of the Wigner function for a mixture of two squeezed displaced states. The Wigner functions are constructed per equations (2.1.18) and (2.1.19) with $\alpha = 5$ and $r = 1/\sqrt{2}$. The characteristic interference fringes and negativity of the Wigner function are apparent in the superposition state.

2.1.2 Fock basis

Mainly for the purpose of future numerical optimization, it is also useful to examine the squeezed cat state in the basis of number states, also called the Fock basis, which consists of eigenkets of the number operator $\hat{N} = \hat{a}^\dagger \hat{a}$ [13]. The coherent state $|\tilde{\alpha}\rangle = \hat{D}(\tilde{\alpha})|0\rangle$ can be written as

$$|\tilde{\alpha}\rangle = e^{-\frac{|\tilde{\alpha}|^2}{2}} \sum_{n=0}^{+\infty} \frac{\tilde{\alpha}^n}{\sqrt{n!}} |n\rangle , \tag{2.1.20}$$

where the general displacement operator

$$\hat{D}(\tilde{\alpha}) \equiv \exp\left(\tilde{\alpha}\hat{a}^\dagger - \tilde{\alpha}^* \hat{a}\right) \tag{2.1.21}$$

is used. This implies that an x displaced state $\hat{D}_x(\alpha')|0\rangle = |\alpha', 0\rangle$ is expressed as

$$|\alpha', 0\rangle = e^{\frac{\alpha'^2}{4}} \sum_{n=0}^{+\infty} \frac{\alpha'^n}{\sqrt{2^n \cdot n!}} |n\rangle \tag{2.1.22}$$

and the superposition of displaced states is thus

$$\frac{1}{\sqrt{2}}\Big(|\alpha', 0\rangle + |-\alpha', 0\rangle\Big) = \frac{e^{-\frac{\alpha'^2}{4}}}{\sqrt{2}} \left(\sum_{n=0}^{+\infty} \frac{\alpha'^n}{\sqrt{2^n \cdot n!}} + \sum_{n=0}^{+\infty} \frac{(-\alpha')^n}{\sqrt{2^n \cdot n!}} \right) |n\rangle , \tag{2.1.23}$$

where the odd terms in the sums cancel out to give

$$\frac{1}{\sqrt{2}}\Big(|\alpha', 0\rangle + |-\alpha', 0\rangle\Big) = \frac{e^{-\frac{\alpha'^2}{4}}}{\sqrt{2}} \sum_{n=0}^{+\infty} \frac{2\alpha'^{2n}}{\sqrt{2^{2n}\,(2n)!}} |2n\rangle . \tag{2.1.24}$$

Notice that by choosing real α', all the coefficients are real. Applying the real squeezing operator $\hat{S}(r')$ from equation (1.2.3) to (2.1.24) keeps all the coefficients real, as its own matrix representation in the Fock basis is just the exponential of $\frac{r}{2}\left(\hat{a}^2 - \hat{a}^{\dagger 2}\right)$, which is a real-valued matrix in the Fock basis. Doing so creates a superposition of displaced-squeezed states, which exist in one-to-one correspondence with squeezed-displaced states [13]. This means that by choosing the correct α', r' for any given α, r we get

$$\begin{aligned} \frac{1}{\sqrt{2}}\hat{S}(r')\Big(|\alpha', 0\rangle + |-\alpha', 0\rangle\Big) &= \hat{S}(r') \left[\frac{e^{-\frac{\alpha'^2}{4}}}{\sqrt{2}} \sum_{n=0}^{+\infty} \frac{2\alpha'^{2n}}{\sqrt{2^{2n}\,(2n)!}} |2n\rangle \right] \\ &= \frac{1}{N_{\alpha,r}}\Big(|\alpha, r\rangle + |-\alpha, r\rangle\Big) = |C_{\alpha,r}\rangle , \end{aligned} \tag{2.1.25}$$

which is a squeezed cat state that has real coefficients in the Fock basis (from the matrix representation of the squeezing operator and (2.1.24)), that are non-zero only for even-numbered Fock states (as the squeezed cat state wave function in x is symmetric, similarly to the superposition of displaced states).

2.2 Important properties

Before proceeding further, let us list some important properties of the squeezed cat state, which follow from the various representations derived in the previous section:

1. the squeezed cat state has symmetric wave functions in x and p,
2. its Wigner function is negative at certain points,
3. its expansion in the Fock basis only contains even terms, which are real-valued,
4. its $p-$representation wave function vanishes at $p = \frac{(2k-1)\pi}{2\alpha}, k \in \mathbb{Z}$.
5. in the limit $r \to +\infty$, the state is invariant under p translations by $\Delta p = \frac{2k\pi}{\alpha}, k \in \mathbb{Z}$,
6. in the limit $r \to +\infty$, the $x-$representation wave function vanishes at $x \neq \pm\alpha$.

Chapter III

Evaluating squeezed cat states

We would like to find a way to evaluate how well a given state approximates the superposition of quadrature eigenkets (1.5.1). We have already established in section 1.4 that the fidelity with any other state is not going to particularly help us, but there are some other methods to consider, which we will introduce generally and then apply to the squeezed cat state in this chapter.

3.1 As virtual interaction resources

One possible way to evaluate how similarly a state behaves to the ideal superposition of quadrature eigenkets is by utilizing it as a resource in an interaction and comparing the resultant output to the ideal output we would expect if we had used the ideal superposition instead.

3.1.1 Quantum nondemolition interaction

An interesting interaction to consider is the Quantum nondemolition interaction (QND interaction), which is a two-mode interaction that ideally transfers all the information from one of the input quadratures into the other mode [27]. QND measurements have been demonstrated experimentally and correspond to so-called sum gates in continuous variable quantum computation [28]. We can describe an ideal QND interaction using the quadrature relations

$$\begin{aligned} \hat{x}_1' &= \hat{x}_1, \qquad & \hat{p}_1' &= \hat{p}_1 - \hat{p}_2, \\ \hat{p}_2' &= \hat{p}_2, \qquad & \hat{x}_2' &= \hat{x}_2 + \hat{x}_1, \end{aligned} \tag{3.1.1}$$

where $\hat{x}_i$ and $\hat{p}_i$ are quadratures of the $i-$th mode described the annihilation operator $\hat{a}_i$ and where the output quadratures are primed. The independent bosonic modes satisfy $\left[\hat{a}_i, \hat{a}_j^\dagger\right] = \delta_{ij}$. We can equivalently describe the interaction using its unitary transformation

$$\hat{U}_{\text{QND}} = \exp\left(-i\hat{x}_1\hat{p}_2\right). \tag{3.1.2}$$

We call $\hat{x}_1$ and $\hat{p}_2$ the nondemolition variables, as they are fully transferred into the output of the other mode while not being affected themselves.

Specifically, we shall consider an interaction depicted in figure 3.1, where the first mode contains the resource state $|\mathrm{R}\rangle$, which will ideally be the superposition of $\hat{x}$ eigenkets defined in (1.5.1), and the second mode contains the vacuum state $|0\rangle$.

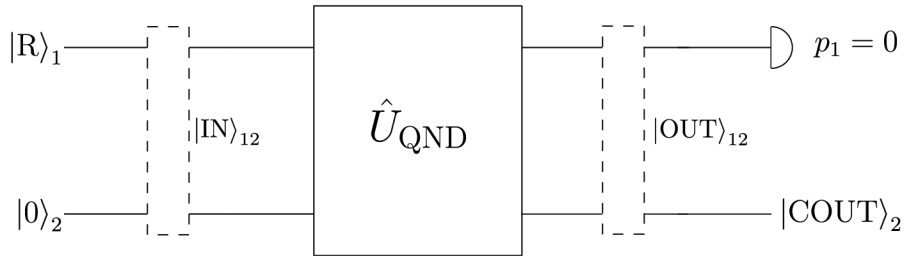

Figure 3.1: Schematic representation of the quantum nondemolition interaction as a unitary black box, time evolution is from left to right, obtaining a conditional output in the second mode is included.

We can write the joint input state of the interaction as

$$|\mathrm{IN}\rangle_{12} = |\mathrm{R}\rangle_1 \otimes |0\rangle_2 = \iint_{-\infty}^{+\infty} \langle x_1|\mathrm{R}\rangle \langle x_2|0\rangle |x_1\rangle_1 \otimes |x_2\rangle_2 \, \mathrm{d}x_1 \, \mathrm{d}x_2, \tag{3.1.3}$$

where $\otimes$ is the tensor product combining the two subsystems (modes) [29]. We use subscripts to specify which mode specific states are associated with. The joint output can be found as

$$|\mathrm{OUT}\rangle_{12} = |\mathrm{OUT1}\rangle_1 \otimes |\mathrm{OUT2}\rangle_2 = \iint_{-\infty}^{+\infty} \langle x_1|\mathrm{R}\rangle \langle x_2|0\rangle |x_1\rangle_1 \otimes |x_1 + x_2\rangle_2 \, \mathrm{d}x_1 \, \mathrm{d}x_2. \tag{3.1.4}$$

We are particularly interested in the output if we measure the first mode p_1 quadrature to be zero. This measurement can be analytically implemented by collapsing the first mode using the ${}_1\langle p_1 = 0|$ eigenbra. We can set ${}_1\langle p_1 = 0| = \int_{-\infty}^{+\infty} {}_1\langle x_3| \, \mathrm{d}x_3$ to obtain the ideal conditional second mode output (up to normalization) as

$$\begin{aligned}
|\mathrm{COUT}_{\mathrm{ideal}}\rangle_2 &= \iiint_{-\infty}^{+\infty} \langle x_1|\mathrm{R}\rangle \langle x_2|0\rangle \langle x_3|x_1\rangle |x_1 + x_2\rangle_2 \, \mathrm{d}x_1 \, \mathrm{d}x_2 \, \mathrm{d}x_3 \\
&= \iint_{-\infty}^{+\infty} \langle x_3|\mathrm{R}\rangle \langle x_2|0\rangle |x_3 + x_2\rangle_2 \, \mathrm{d}x_2 \, \mathrm{d}x_3 \\
&= \iint_{-\infty}^{+\infty} \Big(\langle x_3|x_3 = \alpha\rangle + \langle x_3|x_3 = -\alpha\rangle \Big) \langle x_2|0\rangle |x_3 + x_2\rangle_2 \, \mathrm{d}x_2 \, \mathrm{d}x_3 \\
&= \iint_{-\infty}^{+\infty} \left[\delta(x_3 - \alpha) + \delta(x_3 + \alpha) \right] \langle x_2|0\rangle |x_3 + x_2\rangle_2 \, \mathrm{d}x_2 \, \mathrm{d}x_3 \\
&= \int_{-\infty}^{+\infty} \langle x_2|0\rangle \Big(|x_2 = -\alpha\rangle_2 + |x_2 = \alpha\rangle_2 \Big) \mathrm{d}x_2 \\
&= \int_{-\infty}^{+\infty} \Big[\langle x_2|\hat{D}_{x_2}(-\alpha)|0\rangle + \langle x_2|\hat{D}_{x_2}(\alpha)|0\rangle \Big] |x_2\rangle_2 \, \mathrm{d}x_2 \\
&= \Big[\hat{D}_{x_2}(\alpha) |0\rangle_2 + \hat{D}_{x_2}(-\alpha) |0\rangle_2 \Big].
\end{aligned} \tag{3.1.5}$$

The ideal conditional output is therefore an even superposition of displaced vacuum states centered at eigenvalues corresponding to the resource state eigenkets – a cat state, only this time not a squeezed one. Both of the input states and the conditional output state are visualized using their Wigner functions in figure 3.2.

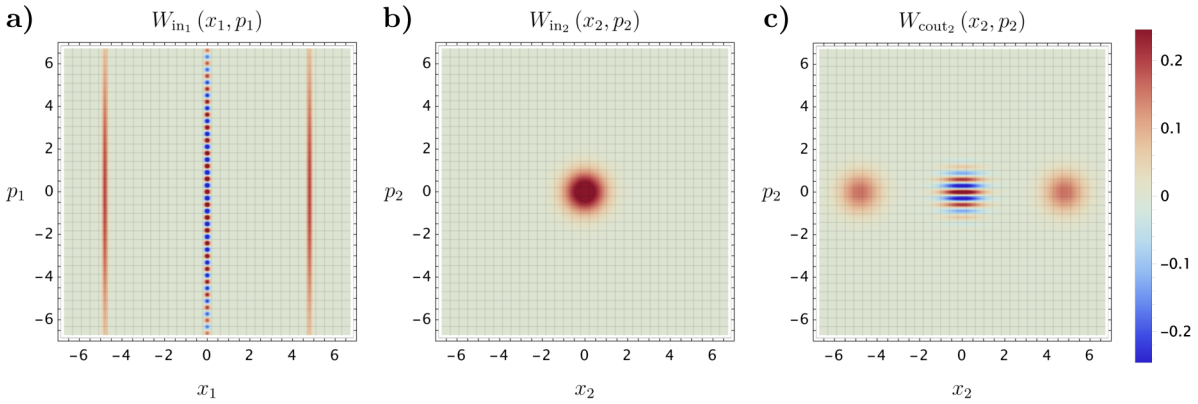

Figure 3.2: Density plots of **a)** the first mode input, **b)** the second mode input and **c)** the conditional second mode output, as given by the QND interaction in figure 3.1 for $\alpha = 5$ and the ideal resource state. Note that the ideal resource state in the first mode input is only approximated by a highly squeezed cat state for the purposes of this visualization.

In order to calculate the conditional output in cases where $|\mathrm{R}\rangle_1$ is a pure state different from the ideal resource, we can pick up on the second line of (3.1.5) and perform a variable substitution $x_2 \to x_2 - x_3$ to obtain

$$|\mathrm{COUT}\rangle_2 = \iint_{-\infty}^{+\infty} \langle x_3|\mathrm{R}\rangle \, \langle x_2|0\rangle \, |x_3 + x_2\rangle_2 \, \mathrm{d}x_2 \, \mathrm{d}x_3 = \iint_{-\infty}^{+\infty} \langle x_3|\mathrm{R}\rangle \, \langle x_2 - x_3|0\rangle \, |x_2\rangle_2 \, \mathrm{d}x_2 \, \mathrm{d}x_3, \tag{3.1.6}$$

which means that the $x-$representation of the (non-normalized) conditional output can be found by simply evaluating the integral

$$\langle x_2|\mathrm{COUT}\rangle = \int_{-\infty}^{+\infty} \langle x_3|\mathrm{R}\rangle \, \langle x_2 - x_3|0\rangle \, \mathrm{d}x_3, \tag{3.1.7}$$

using only the $x-$representations of the resource state and the vacuum state. The nondemolition variable representation of the conditional output is thus simply the convolution of corresponding representations of the interacting states. Performing this integral with the squeezed cat state (1.5.2) as the resource, we obtain the conditional output

$$\langle x_2|\mathrm{COUT}_{\mathrm{cat}}\rangle = \frac{\exp\left(-\frac{e^{2r}\left(2x_2^2 - r + \alpha^2\right) - r}{2(e^{2r}+1)}\right) \cdot \left[\exp\left(\frac{e^{2r}(x_2+\alpha)^2}{2(e^{2r}+1)}\right) + \exp\left(\frac{e^{2r}(x_2-\alpha)^2}{2(e^{2r}+1)}\right)\right]}{\sqrt{2}\sqrt[4]{\pi}\sqrt[4]{e^{2r}+1}\sqrt{e^{\frac{\alpha^2 e^{2r}}{e^{2r}+1}}+1}}. \tag{3.1.8}$$

which quite apparently has the characteristics of a cat state and it converges to the coherent state superposition obtained in (3.1.5) in the resource state squeezing limit of $r \to +\infty$.

The fidelity of this output and the ideal output can be evaluated as

$$F\left(\hat{\rho}_{\mathrm{COUT}_{\mathrm{cat}}}, \hat{\rho}_{\mathrm{COUT}_{\mathrm{ideal}}}\right) = \frac{2e^r\sqrt{e^{2r}+1}\left[\exp\left(\frac{\alpha^2}{2(e^{2r}+1)(2e^{2r}+1)}\right)+\exp\left(\frac{\alpha^2(2e^{2r}+1)}{2(e^{2r}+1)}\right)\right]^2}{\left(e^{\alpha^2}+1\right)\left(2e^{2r}+1\right)\left(e^{\frac{\alpha^2 e^{2r}}{e^{2r}+1}}+1\right)} \tag{3.1.9}$$

and plotted as a function of α, r, see figure 3.3. It is apparent that $F > 0.9$ can be achieved even with zero squeezing, which is quite interesting. It seems that a superposition of $x-$displaced states is itself a decent approximation for a superposition of $x-$eigenkets, but we can also see that the fidelity increases significantly when squeezing is introduced, although it cannot reach unity for any physical state. Notice that there is a visible irregularity for small values of α and small squeezing, which can be attributed to the constituent states of both the resource and the output superpositions partially overlapping (picture the rightmost state in figure 3.2 with $\alpha \in [1, 2]$), which results in the fidelity function taking on a more interesting shape there.

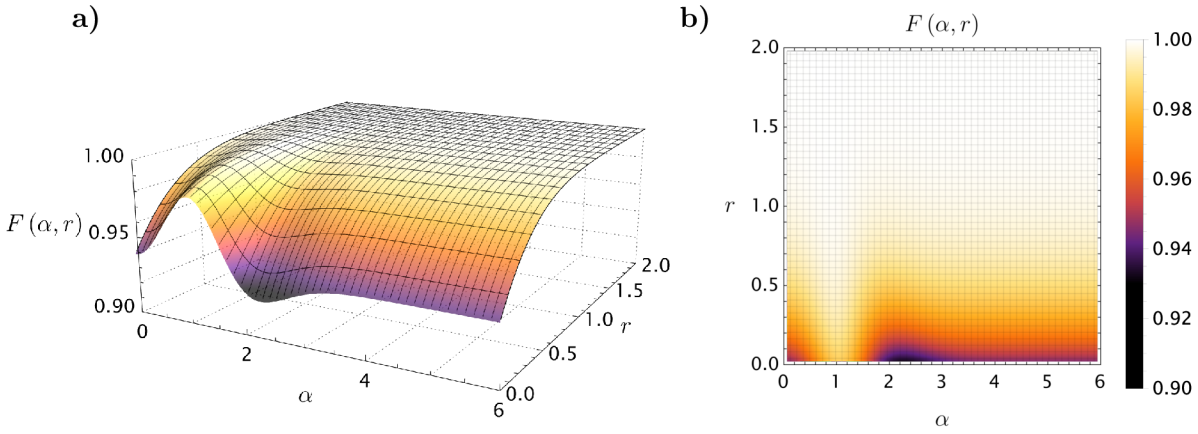

Figure 3.3: **a)** 3D plot and **b)** density plot of the fidelity of the ideal QND measurement conditional output obtained using a superposition of $x-$eigenkets and the realistic output obtained using a squeezed cat state as a function of α and r.

It should also be mentioned that while we may have criticized fidelity in the first chapter, in this case, we are using it to compare two normalizable superpositions and not trying to target any unphysical states – the variance ratio issue outlined in section 1.4 is therefore irrelevant to this case.

3.1.2 Beam splitter

A conceptually slightly simpler interaction to consider is an interaction of the squeezed cat state and the vacuum in a beam splitter. The ideal beam splitter interaction can be described by the unitary transformation [20]

$$\hat{U}_{\mathrm{BS}} = \exp\left[-\theta\left(\hat{a}_1^\dagger \hat{a}_2 - \hat{a}_2^\dagger \hat{a}_1\right)\right], \tag{3.1.10}$$

where θ can be intuitively connected with the transmission and reflection coefficients of the beam splitter as $|T| = \cos\theta, |R| = \sin\theta$. It is useful to express the unitary transformation using mode quadratures as

$$\hat{U}_{\mathrm{BS}} = \exp\left[i\theta\left(\hat{p}_1\hat{x}_2 - \hat{p}_2\hat{x}_1\right)\right], \tag{3.1.11}$$

which is an evolution operator associated with the Hamiltonian $\hat{H} = \hat{p}_2\hat{x}_1 - \hat{p}_1\hat{x}_2$. We can therefore solve Heisenberg's equations of motion [11] to obtain the output quadratures as functions of θ:

$$\begin{aligned} \hat{x}_1' &= \hat{x}_1\cos\theta + \hat{x}_2\sin\theta, & \hat{p}_1' &= \hat{p}_1\cos\theta + \hat{p}_2\sin\theta, \\ \hat{p}_2' &= \hat{p}_2\cos\theta - \hat{p}_1\sin\theta, & \hat{x}_2' &= \hat{x}_2\cos\theta - \hat{x}_1\sin\theta. \end{aligned} \tag{3.1.12}$$

We will again follow the same setup as before, only replacing the unitary transformation for one of the beam splitter. The interaction is visualized in figure 3.4.

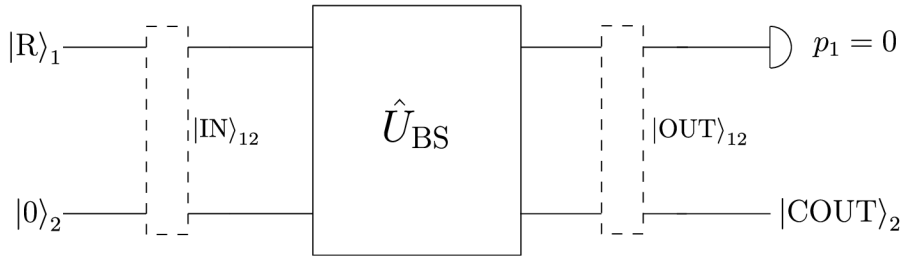

Figure 3.4: Schematic representation of the beam splitter interaction as a unitary black box, time evolution is from left to right, obtaining a conditional output in the second mode is included.

Specifically, we shall consider a 50:50 beam splitter with $\theta = \pi/4$. The joint output after the beam splitter transformation is

$$|\mathrm{OUT}\rangle_{12} = \iint_{-\infty}^{+\infty} \langle x_1|\mathrm{R}\rangle \langle x_2|0\rangle \left|\frac{x_1+x_2}{\sqrt{2}}\right\rangle_1 \otimes \left|\frac{x_2-x_1}{\sqrt{2}}\right\rangle_2 \mathrm{d}x_1\,\mathrm{d}x_2 \tag{3.1.13}$$

per (3.1.12), and the conditional second mode output for $p_1 = 0$ is

$$\begin{aligned} |\mathrm{COUT}\rangle_2 &= \iiint_{-\infty}^{+\infty} \langle x_1|\mathrm{R}\rangle \langle x_2|0\rangle \left\langle x_3\middle|\frac{x_1+x_2}{\sqrt{2}}\right\rangle \left|\frac{x_2-x_1}{\sqrt{2}}\right\rangle_2 \mathrm{d}x_1\,\mathrm{d}x_2\,\mathrm{d}x_3 \\ &= \iint_{-\infty}^{+\infty} \left\langle x_3\sqrt{2} - x_2\middle|\mathrm{R}\right\rangle \langle x_2|0\rangle \left|x_2\sqrt{2} - x_3\right\rangle_2 \mathrm{d}x_2\,\mathrm{d}x_3 \\ &= \iint_{-\infty}^{+\infty} \left\langle \frac{x_3-x_2}{\sqrt{2}}\middle|\mathrm{R}\right\rangle \left\langle \frac{x_2+x_3}{\sqrt{2}}\middle|0\right\rangle |x_2\rangle_2\,\mathrm{d}x_2\,\mathrm{d}x_3, \end{aligned} \tag{3.1.14}$$

where we performed the substitution $x_2\sqrt{2} - x_3 \to x_2$ in the last line and ignored the renormalization going with it, as the states are not normalized either way, due to the act of measurement in one of the modes. We expect the ideal output to be the infinite squeezing limit of the squeezed cat output, so let us compute that one first

$$\begin{aligned}\langle x_2|\mathrm{COUT}_{\mathrm{cat}}\rangle = &\frac{\exp\left(-\frac{e^{2r}\left(4x_2^2-r+\alpha^2\right)-r}{2\left(e^{2r}+1\right)}\right)}{\sqrt[4]{2}\sqrt[4]{\pi}\sqrt[4]{e^{2r}+1}\sqrt{e^{\frac{\alpha^2 e^{2r}}{e^{2r}+1}}+1}}\\ &\times\left[\exp\left(\frac{e^{2r}\left(4x_2^2+2^{\frac{5}{2}}\alpha x_2+2\alpha^2\right)}{4\left(e^{2r}+1\right)}\right)+\exp\left(\frac{e^{2r}\left(4x_2^2-2^{\frac{5}{2}}\alpha x_2+2\alpha^2\right)}{4\left(e^{2r}+1\right)}\right)\right].\end{aligned} \tag{3.1.15}$$

In the limit $r \to +\infty$ we get

$$\langle x_2|\mathrm{COUT}_{\mathrm{ideal}}\rangle = \frac{e^{-\frac{-\alpha^2-\frac{\ln(2)}{2}}{2}}}{\sqrt{2}\sqrt[4]{\pi}\sqrt{e^{\alpha^2}+1}}\cdot\left[\exp\left(-\left(x+\frac{\alpha}{\sqrt{2}}\right)^2\right)+\exp\left(-\left(x-\frac{\alpha}{\sqrt{2}}\right)^2\right)\right], \tag{3.1.16}$$

which can be written as a squeezed cat state with specific parameters or as a squeezed superposition of coherent states

$$\begin{aligned}|\mathrm{COUT}_{\mathrm{ideal}}\rangle = \left|C_{\alpha/\sqrt{2},\ln 2/2}\right\rangle &= \frac{1}{N_{\alpha/\sqrt{2},\ln 2/2}}\left[\hat{D}_x\left(\frac{\alpha}{\sqrt{2}}\right)+\hat{D}_x\left(-\frac{\alpha}{\sqrt{2}}\right)\right]\hat{S}\left(\frac{\ln 2}{2}\right)|0\rangle\\ &= \frac{1}{N_{\alpha/\sqrt{2},\ln 2/2}}\hat{S}\left(\frac{\ln 2}{2}\right)\left[\hat{D}_x(\alpha)+\hat{D}_x(-\alpha)\right]|0\rangle\,.\end{aligned} \tag{3.1.17}$$

The interaction inputs and conditional output are visualized in figure 3.5. The conditional output is slightly squeezed compared to the QND interaction output from figure 3.2.

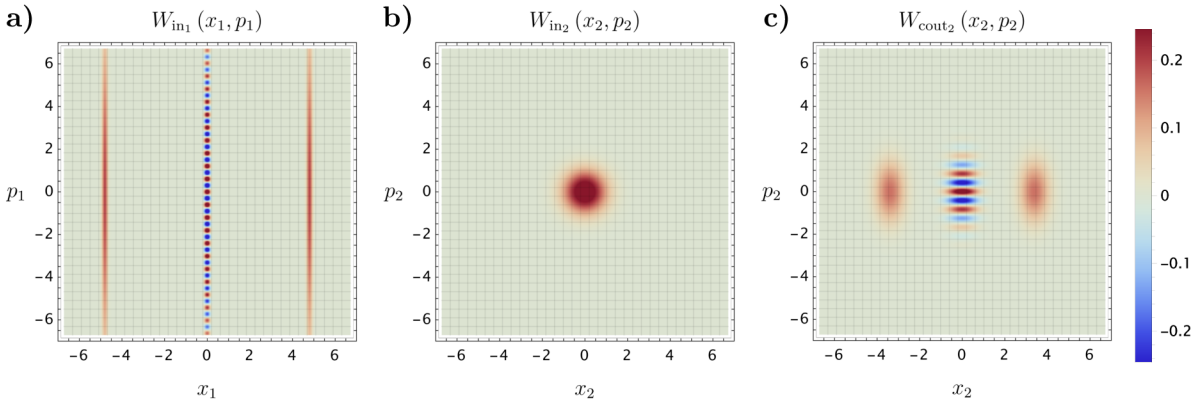

Figure 3.5: Density plots of **a)** the first mode input, **b)** the second mode input and **c)** the conditional second mode output, as given by the considered beam splitter interaction for $\alpha = 5$ and the ideal resource state. Note that the ideal resource state in the first mode input is only approximated by a highly squeezed cat state for the purposes of this visualization.

We can again calculate the fidelity of the real output and the ideal output as

$$F\left(\hat{\rho}_{\mathrm{COUT}_{\mathrm{cat}}}, \hat{\rho}_{\mathrm{COUT}_{\mathrm{ideal}}}\right) = \frac{2e^r\sqrt{e^{2r}+1}\left[\exp\left(\frac{\alpha^2}{2(e^{2r}+1)(2e^{2r}+1)}\right)+\exp\left(\frac{\alpha^2\cdot\left(2e^{2r}+1\right)}{2(e^{2r}+1)}\right)\right]^2}{\left(e^{\alpha^2}+1\right)\left(2e^{2r}+1\right)\left(e^{\frac{\alpha^2 e^{2r}}{e^{2r}+1}}+1\right)}, \quad (3.1.18)$$

which is exactly the same result we obtained for the QND interaction. For the squeezed cat state, both of these methods give us the same information, but that is not the case for all states (as will be seen later). For thoroughness, the fidelity is again plotted in figure 3.6.

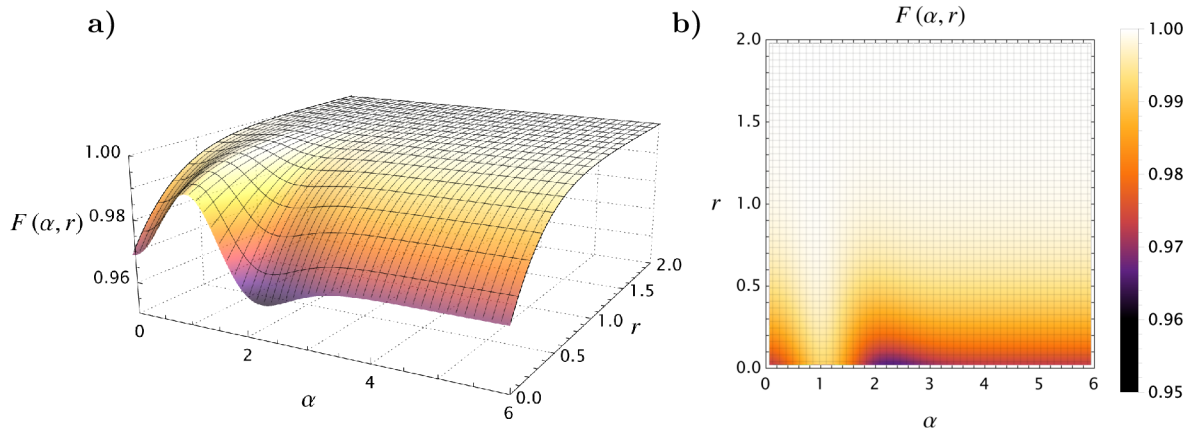

Figure 3.6: **a)** 3D plot and **b)** density plot of the fidelity of the ideal beam splitter measurement conditional output obtained using a superposition of $x-$eigenkets and the realistic output obtained using a squeezed cat state as a function of α and r.

3.2 By measuring an observable

We have shown that $x-$eigenket superpositions behave in a certain way when interacting with the vacuum state, and that one possible way of evaluating the quality of a given state as an approximation of said eigenket superposition is to perform the same interaction with the given state and compare the output with the ideal output by means of quantum state fidelity. This is a straightforward and intuitive way to approach this problem; however, its realization is not necessarily practical, as both the interaction and subsequent measurements have to be performed to be able to determine the fidelity (either numerically or experimentally). We have also not shown whether any local interaction fidelity maxima exist and whether the states that behave like quadrature eigenket superpositions in the aforementioned interactions necessarily share their structure as well. In order to do so, introducing a different method is desirable.

The goal of this section is to find a quantity that can be measured directly from the quantum state we want to evaluate, and ideally provides similar information to the interaction-based methods. A simple way to obtain at least a theoretically measurable quantity, is to consider hermitian operators and their expectation values, which are by definition real-valued [11].

3.2.1 Eigenvalue operators

Let us now return to the squeezed cat state properties listed in section 2.2. We are particularly interested in the properties for the limit of large squeezing, as we ideally want the state to have identical properties to an eigenket superposition. We only want the quadrature eigenvalues of $x = \pm\alpha$ to be measurable, and it is quite easy to design an operator with a minimized expectation value for that case. Consider

$$\hat{O}_1(\alpha) \equiv \left(\hat{x}^2 - \alpha^2\right)^2. \tag{3.2.1}$$

Applying this operator in the $x-$representation simply amounts to multiplying the wavefunction by $\left(x^2 - \alpha^2\right)^2$, which is a function positive everywhere except for $x = \pm\alpha$, where its value is zero. This means that in order for $\left\langle \hat{O}_1 \right\rangle$ to be zero, the $x-$representation wavefunction of the state has to be fully localized at $x = \pm\alpha$ and an $x-$eigenket superposition thus minimizes this operator. It is unfortunately not the only state minimizing this operator, as we have already established in section 2.1 that an equal mixture of $x-$eigenkets at $\pm\alpha$ is also going to minimize this operator, and that, in general, no operator based solely on $\hat{x}$ can suffice.

Another valid criticism of 3.2.1 would be that it does not give the same weight to both sides of the peaks. By that we mean the fact that $\left(x^2 - \alpha^2\right)^2$ grows faster for $|x| > \alpha$ than for $|x| < \alpha$ and it also diverges to infinity in the first case, while only getting up to α^4 at zero. We would ideally like for the function to grow the same way going both directions from $\pm\alpha$, so that we prioritize symmetric peaks while minimizing the operator expectation value and do not get approximate states with peaks "heavier" on one side. This is not really possible to achieve, as making the operator diverge at zero would make it non-hermitian. It would be possible to solve this problem through evaluating the variance around both α and $-\alpha$ separately by dividing the wavefunction into two parts for $x > 0$ and $x < 0$, but this again does not align with our goal of finding one hermitian operator.

To ensure that the studied state is a superposition and not a mixture, we need to consider a property that only occurs in superposition states. We have shown that in a pure squeezed cat state (no matter the squeezing) the $p-$representation wave function vanishes at $p = \frac{(2k-1)\pi}{2\alpha}$ for $k \in \mathbb{Z}$. This is basically the opposite of the situation in the $x-$basis, where only specific eigenvalues can be measured. In order to detect this behavior using an operator, we would like it to correspond to a function of p that is zero everywhere, except for the vanishing eigenvalues. One way to achieve this, is to simply consider projections onto the eigenvalues

$$\hat{O}_2(\alpha) \equiv \sum_{k=-\infty}^{+\infty} \left| p = \frac{(2k-1)\,\pi}{2\alpha} \right\rangle \left\langle p = \frac{(2k-1)\,\pi}{2\alpha} \right|. \tag{3.2.2}$$

The expectation value of this operator is zero for pure cat states and greater than zero for any state that contains non-zero values at $p = \frac{(2k-1)\pi}{2\alpha}$ in its $p-$representation. It does not give us any information about the squeezing, as we have established that this is a property of all squeezed cat states.

Note that this operator can be approximated as a harmonic function[1] up to normalization

$$\hat{O}_2'(\alpha) = \lim_{z\to+\infty} [\sin(\alpha\hat{p})]^{2z} = \lim_{z\to+\infty} \left(-\frac{1}{4}\right)^z [\exp(-i\alpha\hat{p}) - \exp(i\alpha\hat{p})]^{2z}, \tag{3.2.3}$$

which is essentially an infinite product of inverse $x-$displacement operator combinations. Using this representation, we can also approximate this operator by choosing large z, which is quite useful for numerical methods, as eigenket projections from equation (3.2.2) are not available in a finite Fock basis. We can combine the two introduced operators to get

$$\hat{O}(\alpha) = \hat{O}_1(\alpha) + \hat{O}_2(\alpha), \tag{3.2.4}$$

which should allow $\left\langle \hat{O}(\alpha) \right\rangle = 0$ only for an infinitely squeezed cat state with displacement α, i.e. the superposition of $x-$eigenkets, and greater expectation values for all other states. We can explicitly evaluate $\left\langle \hat{O}(\alpha) \right\rangle$ for a squeezed cat state by using the wave functions in (2.1.2) and (2.1.10) to obtain

$$\left\langle \hat{O}(\alpha) \right\rangle = \frac{\frac{4e^{2r}\left(e^{2r}\alpha^2-3\right)}{e^{e^{2r}\alpha^2}+1} + 8e^{2r}\alpha^2 + 3}{4e^{4r}}, \tag{3.2.5}$$

which is decreasing everywhere as a function of r and converges to zero in the limit of $r \to +\infty$, exactly as expected. We further expect that the lower the value of $\left\langle \hat{O}(\alpha) \right\rangle$ is, the more the state behaves like an ideal superposition of eigenkets, however, this cannot be confirmed without a thorough numerical analysis, which is performed in the following chapter.

3.2.2 Detecting decoherence

In the rest of the thesis, we will mainly resort to numerical methods to fully evaluate the proposed quality measures. For the final purely analytical part, however, we can test how well the proposed operators detect decoherence of squeezed cat states. All physical systems undergo losses [13] and losses are the most common source of decoherence in optical superpositions, as they are associated with the loss of correlation between the constituent states.

We can understand decoherence as the process during which a squeezed cat state turns into a mix of squeezed displaced states through the loss of interference fringes, refer to figure 2.2 for visualization. It can be argued that while curiosity gets the cat into the box, it is decoherence that truly kills it. Further losses then push the previously superposed states together, eventually resulting in a vacuum (or thermal) state. Losses are often modeled stochastically using the master equation, which is derived by coupling the electromagnetic mode to a heat bath [13]. In the interaction picture, we can write the master equation as

$$\dot{\hat{\rho}} = \frac{\Gamma}{2} N L\left[\hat{a}^\dagger\right]\hat{\rho} + \frac{\Gamma}{2}(N+1) L[\hat{a}]\hat{\rho} - \frac{\Gamma}{2}\left(M^* D[\hat{a}]\hat{\rho} + M D\left[\hat{a}^\dagger\right]\hat{\rho}\right), \tag{3.2.6}$$

where $\Gamma > 0$ is the damping constant, $M = M_1 + iM_2$ is a complex number called the squeezing of the bath, which is zero at thermal equilibrium, N is a parameter related to the purity of the

[1] The even exponent $2z$ is chosen in order to make the function non-negative everywhere.

asymptotic state (and to the number of thermal photons in the bath), and $L\left[\hat{O}\right]$ and $D\left[\hat{O}\right]$ are the Lindblad superoperators [17]

$$L\left[\hat{O}\right]\hat{\rho} \equiv 2\hat{O}\hat{\rho}\hat{O}^{\dagger} - \hat{O}^{\dagger}\hat{O}\hat{\rho} - \hat{\rho}\hat{O}^{\dagger}\hat{O}, \tag{3.2.7}$$

$$D\left[\hat{O}\right]\hat{\rho} \equiv 2\hat{O}\hat{\rho}\hat{O} - \hat{O}\hat{O}\hat{\rho} - \hat{\rho}\hat{O}\hat{O}. \tag{3.2.8}$$

We will not go into detail of how the master equation is actually solved, as open quantum systems are outside the scope of this work. The important fact is that it can be analytically solved for the squeezed cat state in the phase space representation. In the idealized case of $M = N = 0$, which corresponds to a state at equilibrium with a zero temperature bath [13], we obtain the squeezed cat Wigner function time evolution as [17]

$$\begin{aligned}
&W_{\text{cat}}(x,p,t) = \\
&\frac{e^{t\Gamma+r}\left(\frac{e^{t\Gamma+4r}}{4} - \frac{e^{t\Gamma+2r}}{2} + \frac{e^{2(t\Gamma+r)}}{4} + \frac{e^{t\Gamma}}{4} - \frac{e^{4r}}{4} + \frac{e^{2r}}{2} - \frac{1}{4}\right)^{-\frac{1}{2}}}{4\pi\left(e^{-\alpha^2(\sinh(r)+\cosh(r))^2}+1\right)} \times \Bigg\{ e^{-\alpha^2(\sinh(r)+\cosh(r))^2} \\
&\times \Bigg[e^{-\frac{i\left(e^{t\Gamma}\left(e^{2r}\left(ie^{t\Gamma}+ie^{2r}-i\right)x^2+p^2\left(ie^{t\Gamma+2r}-ie^{2r}+i\right)\right)+\alpha^2\left(-ie^{t\Gamma+6r}+ie^{6r}-ie^{4r}\right)+\alpha p e^{\frac{t\Gamma}{2}+2r}\left(-2e^{t\Gamma+2r}+2e^{2r}-2\right)\right)}{(-e^{t\Gamma}-e^{2r}+2)e^{t\Gamma+2r}-e^{t\Gamma}+e^{4r}-2e^{2r}+1}} \\
&+ e^{\frac{e^{t\Gamma}\left(e^{2r}\left(-e^{t\Gamma}-e^{2r}+1\right)x^2+p^2\left(-e^{t\Gamma+2r}+e^{2r}-1\right)\right)+\alpha^2\left(e^{t\Gamma+6r}-e^{6r}+e^{4r}\right)+\alpha p e^{\frac{t\Gamma}{2}+2r}\left(2ie^{t\Gamma+2r}-2ie^{2r}+2i\right)}{e^{t\Gamma+4r}-2e^{t\Gamma+2r}+e^{2(t\Gamma+r)}+e^{t\Gamma}-e^{4r}+2e^{2r}-1}} \Bigg] \\
&+ e^{\frac{e^{t\Gamma}\left(e^{2r}\left(-e^{t\Gamma}-e^{2r}+1\right)x^2+p^2\left(-e^{t\Gamma+2r}+e^{2r}-1\right)\right)+\alpha\left(2e^{t\Gamma}+2e^{2r}-2\right)e^{\frac{t\Gamma}{2}+2r}x+\alpha^2e^{2r}\left(-e^{t\Gamma}-e^{2r}+1\right)}{e^{t\Gamma+4r}-2e^{t\Gamma+2r}+e^{2(t\Gamma+r)}+e^{t\Gamma}-e^{4r}+2e^{2r}-1}} \\
&+ e^{\frac{e^{t\Gamma}\left(e^{2r}\left(-e^{t\Gamma}-e^{2r}+1\right)x^2+p^2\left(-e^{t\Gamma+2r}+e^{2r}-1\right)\right)+\alpha\left(-2e^{t\Gamma}-2e^{2r}+2\right)e^{\frac{t\Gamma}{2}+2r}x+\alpha^2e^{2r}\left(-e^{t\Gamma}-e^{2r}+1\right)}{e^{t\Gamma+4r}-2e^{t\Gamma+2r}+e^{2(t\Gamma+r)}+e^{t\Gamma}-e^{4r}+2e^{2r}-1}} \Bigg\}.
\end{aligned} \tag{3.2.9}$$

This expression represents an analytical solution of the squeezed cat state loss and allows us to evaluate expectation values at any time for any operator we can find the Weyl transform of. This is not really a problem – if we can write an operator as a sum of operators that are dependent solely on $\hat{x}$ or solely $\hat{p}$, then the Weyl transform of such operator is obtained simply by replacing $\hat{x}, \hat{p}$ for x, p [26]. All operators mentioned so far are of this form.

Note that in the zero-temperature case, the state converges to the vacuum as $t \to +\infty$, as opposed to a general thermal state for any $N > 0$, this is luckily the optical default. Also note that while there are complex numbers present in (3.2.9), the function is real-valued as the summed pairs of exponentials are derived from complex conjugate matrix exponentials [17].

We can now study how expectation values for operators introduced in this section evolve with losses using the analytical solution obtained in (3.2.9), the general phase-space expectation value (2.1.17) and the trivial Weyl transforms of the studied operators. The solutions for $\Gamma = 1$ are plotted in figure 3.7.

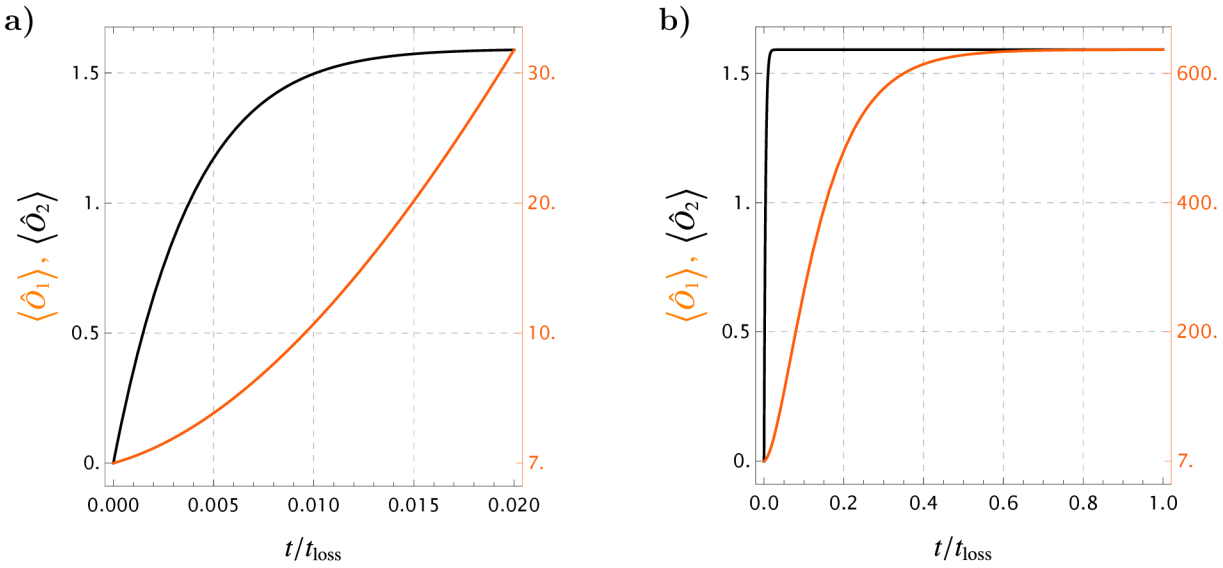

Figure 3.7: Time evolution of $\left\langle \hat{O}_1(\alpha) \right\rangle$ and $\left\langle \hat{O}_2(\alpha) \right\rangle$ plotted in two different time scales, plot **a)** shows initial decoherence, where interference fringes are lost, plot **b)** shows the entire loss process with convergence to the vacuum state. A squeezed cat state with $\alpha = 5, r = 1$ and losses governed by equation (3.2.6) with $N = M = 0, \Gamma = 1$ were chosen, axes are assigned by color, t_{loss} is the time at which the quantum state converges to the vacuum (within used precision).

We can see that both operators do what we expect them to: $\hat{O}_2(\alpha)$ detects the loss of correlation between constituent states, which happens quite quickly, whereas $\hat{O}_1(\alpha)$ increases as the states lose energy until only the vacuum state is left, which takes much longer. The operator $\hat{O}(\alpha)$ thus detects both of these distinct phases of loss.

A question that arises naturally upon looking at the axis values in figure 3.7, is whether it is wise to give both of these operators the same weight as we had done in (3.2.4). Unfortunately, this question does not have a good answer because the values of $\left\langle \hat{O}_2(\alpha) \right\rangle$ are bounded, whereas that is not the case for $\left\langle \hat{O}_1(\alpha) \right\rangle$. Determining an appropriate weight for $\hat{O}_2(\alpha)$ is thus a problem, which does not seem to have a unique solution. In general, we can consider operators of the form

$$\hat{O}_c(\alpha, c) = \hat{O}_1(\alpha) + c \cdot \hat{O}_2(\alpha), \qquad c > 0, \tag{3.2.10}$$

$$\hat{O}_\omega(\alpha, \omega) = \hat{O}_1(\alpha) \cos\omega + \hat{O}_2(\alpha) \sin\omega, \qquad \omega \in [0, 2\pi], \tag{3.2.11}$$

where the parameter c or ω can be chosen depending on the specific application. Note that while equation (3.2.11) allows for operators which are not positive semi-definite and is not generally minimized for the even eigenket superposition, it could still be an interesting object to study in the context of superpositions of squeezed states. In this work, however, we are mostly interested in obtaining the eigenket superpositions and will therefore continue focusing only on the positive semi-definite operator (3.2.10) with $c = 1$.

Chapter IV

Numerical analysis

We have proposed three distinct ways to evaluate the suitability of quadrature eigenket superposition approximations in the last chapter – two interaction based and one operator based measure. So far, we have mostly applied them to the model of the squeezed cat state (1.5.2). This state turned out to be a perfect approximation in the limit of high squeezing and a highly squeezed cat state is realistically the most we can hope to achieve, but only considering states of this very specific form will not get us too far.

In this section, we shall utilize numerical optimization in truncated Fock spaces to explore more complex quantum states in order to find out if the proposed methods actually agree with each other, and determine how much information they convey and what their limitations are.

4.1 Truncated Fock basis approximations

It has been established in the first chapter that the spectra of quadrature operators are continuous and unbounded. Therefore, if we want to consider all possibilities in spaces spanned by these operators, we run into the problem of having an infinite number of parameters. Limiting their amount is thus crucial to perform any numerical calculations and there are multiple ways of doing so. A reasonable one, however, is to consider the first m eigenstates of the number operator, which form the truncated Fock basis

$$\{|n\rangle\} = \{|0\rangle, |1\rangle, \ldots, |m-1\rangle\}. \tag{4.1.1}$$

This way, we limit ourselves to $2m-2$ parameters[1] for pure states and generally work in an $m-$dimensional Hilbert space obtained as the span of this basis. All operators derived from the bosonic annihilation operator can also be written in the Fock basis because the annihilation operator functions as a lowering operator in this basis, following the fundamental relation [10]

$$\hat{a}\,|n\rangle = \sqrt{n}\,|n-1\rangle, \tag{4.1.2}$$

[1]There are m complex coefficients, the normalization requirement and global phase.

which implies that in the Fock basis, it can be written as

$$\hat{a} = \begin{pmatrix} 0 & \sqrt{1} & 0 & 0 & \dots \\ 0 & 0 & \sqrt{2} & 0 & \dots \\ 0 & 0 & 0 & \sqrt{3} & \dots \\ \vdots & \vdots & \vdots & \vdots & \ddots \end{pmatrix}. \tag{4.1.3}$$

This representation is sufficient to derive the Fock basis forms of the quadrature operators, the squeezing operator, and the displacement operator, as all of these have been established to be functions of the annihilation operator in the first chapter. Obtaining the truncated Fock basis representations is then done either by simply discarding all matrix elements for $n > m-1$ in the infinite-dimensional operator, or by using its relation to the annihilation operator with the truncated form of $\hat{a}$ plugged in. These representations are generally different and associated with differing errors [30]. In this work, we will utilize the second method.

In order to determine whether a state is well approximated in the given truncated Fock basis (i.e. similar to its representation in an infinite-dimensional Fock space), we have designed a simple criterion. Consider a state $|A_m\rangle$ in the $m-$dimensional Fock basis

$$|A_m\rangle = \hat{\Omega}\left(\hat{a}_m\right)|0\rangle\,, \tag{4.1.4}$$

where $\hat{\Omega}$ is an operator function of the $m-$dimensional annihilation operator.[2] Notice that all the states we worked with so far are actually of this form. We will say that $|A_m\rangle$ is well approximated in the $m-$dimensional basis, if the state

$$|B_{10m}\rangle = \hat{\Omega}\left(\hat{a}_{10m}\right)|0\rangle\,, \tag{4.1.5}$$

which is a different state created using the same operator in a higher-dimensional representation, has the property

$$\sum_{n=0}^{m-1} |\langle n|B_{10m}\rangle|^2 \geq 0.99. \tag{4.1.6}$$

This criterion says that a state is well approximated in an $m-$dimensional Fock space if a state created using the same operators in a $10m-$dimensional Fock space has $\geq 99\,\%$ probability of measuring $n = 0, \dots, m-1$ in the number basis. We expect $|B_{10m}\rangle$ to be practically identical to the infinite-dimensional case obtained using the exact form of $\hat{\Omega}$, this criterion therefore tells us, that even the infinite-dimensional state is predominantly composed of Fock states with $n < m$.

Note that both the probability ($99\,\%$) and the dimensional expansion ($10\times$) are a matter of choice. This specific combination of values was chosen as the Wigner functions of well-approximated states per criterion (4.1.6) were close to indistinguishable from Wigner functions of their infinite-dimensional representations. Choosing a lower probability, for example, resulted

[2] The `QuTiP` library [31] also obtains its truncated operators by simply using their relation to the annihilation operator and plugging in its truncated form, it is therefore natural to study the $\hat{\Omega}\left(\hat{a}_m\right)$ operator.

in well-approximated states containing clearly visible fringes in their Wigner functions (which do not appear in the infinite-dimensional case).

4.2 Optimization

Let us now examine the operator $\hat{O}(\alpha)$ introduced in (3.2.4). It can be implemented in a truncated Fock space quite easily; $\hat{O}_1(\alpha)$ can be obtained directly using the $\hat{x}$ operator and $\hat{O}_2(\alpha)$ can be implemented through its approximation in (3.2.3) using the displacement operator. We have chosen $z = 500$, as using greater values of z resulted in the number system overflowing and returning ∞ in certain coefficients. We propose two ways of finding the quantum state that minimizes the expectation value of an operator with non-negative eigenvalues:

4.2.1 Eigenvalue minimization

The more efficient way to find the optimal state is by simply finding the eigenstate of the operator with the lowest eigenvalue. All possible expectation values for an operator must be bound by its eigenvalues, as any state can be written in the eigenstate basis. The state with minimized expectation value of an operator with non-negative eigenvalues can therefore be found by selecting the ground state of the operator. The Python code to do this is shown in A.1. Results of this optimization for $\left\langle \hat{O}(\alpha) \right\rangle$ in two different truncated Fock bases are visualized in figures 4.1 and 4.2, where the optimized states are compared with the most squeezed, well approximated cat states (per criterion (4.1.6)) in the given Fock basis (found using A.2).

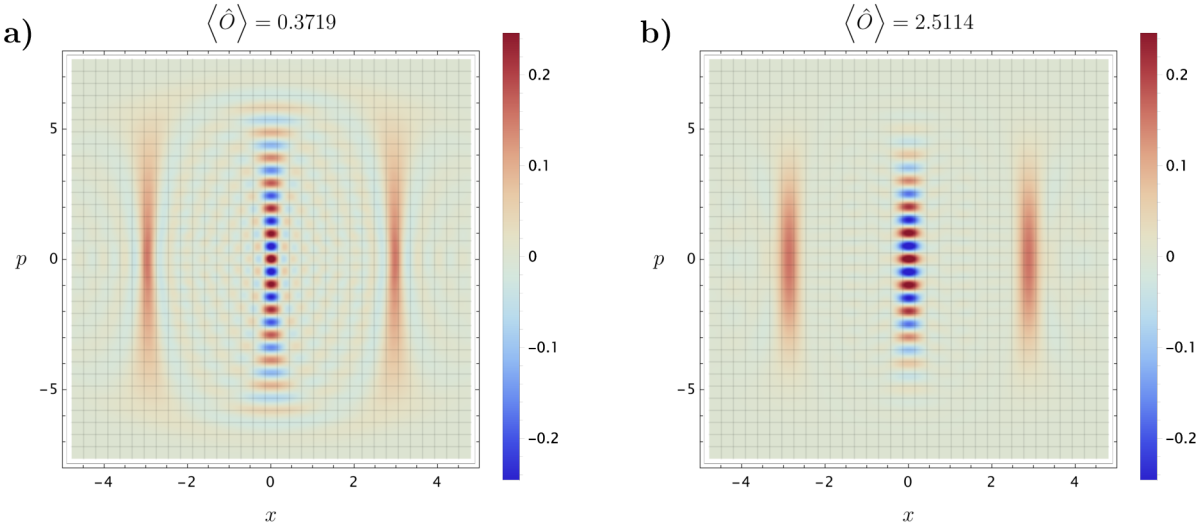

Figure 4.1: Wigner functions of **a)** the state with minimal $\left\langle \hat{O}(\alpha) \right\rangle$ and **b)** the most squeezed cat state available in the truncated Fock basis (per criterion (4.1.6)) for dimension $m = 30$ and displacement $\alpha = 3$. The corresponding expectation values are denoted above the plots, both of the Wigner functions are constructed only using Fock states with eigenvalues $n \leq m - 1$.

It is apparent that the state obtained using eigenvalue minimization returns a lower expectation value than the most squeezed cat state available in the truncated Fock basis according to our criterion. The minimum eigenvalue state indeed looks very much like a squeezed cat state and it also possess its properties, like having nonzero coefficients only for even-numbered Fock states, with those coefficients also being real (see section 2.2). Here, these properties arise naturally by minimizing $\left\langle \hat{O}(\alpha) \right\rangle$, as does Wigner function negativity and symmetry.

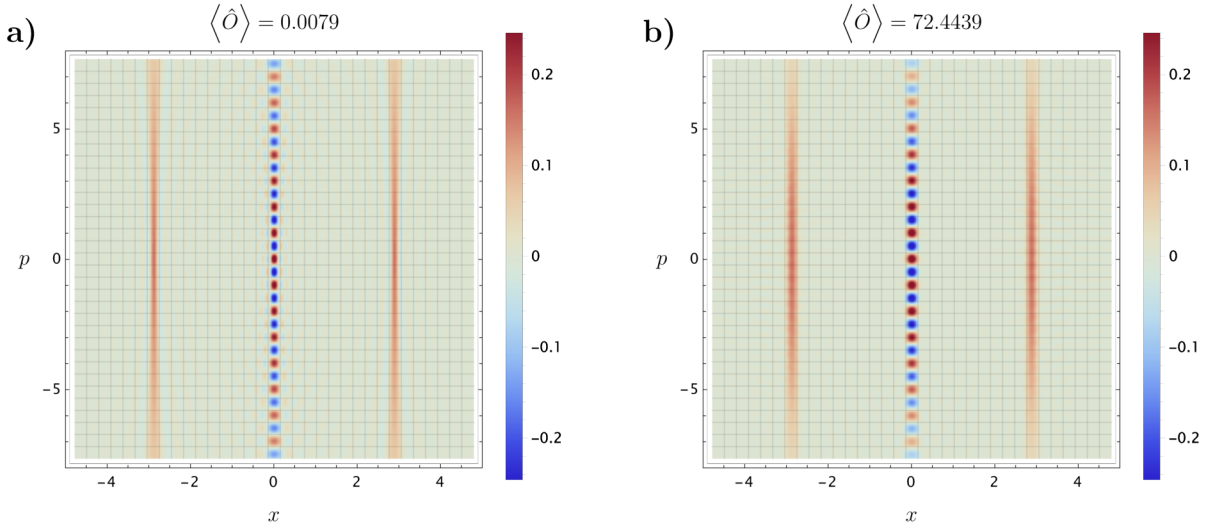

Figure 4.2: Wigner functions of **a)** the state with minimal $\left\langle \hat{O}(\alpha) \right\rangle$ and **b)** the most squeezed cat state available in the truncated Fock basis (per criterion (4.1.6)) for dimension $m = 100$ and displacement $\alpha = 3$. The corresponding expectation values are denoted above the plots, both of the Wigner functions are constructed only using Fock states with eigenvalues $n \leq m - 1$.

One issue with truncated Fock spaces is the fact that the smallest available eigenvalue is highly dependent on the dimension m and displacement α. To quantify this problem, we have plotted minimum $\hat{O}(\alpha)-$eigenvalue dependence on m for three different displacements in figure 4.3.

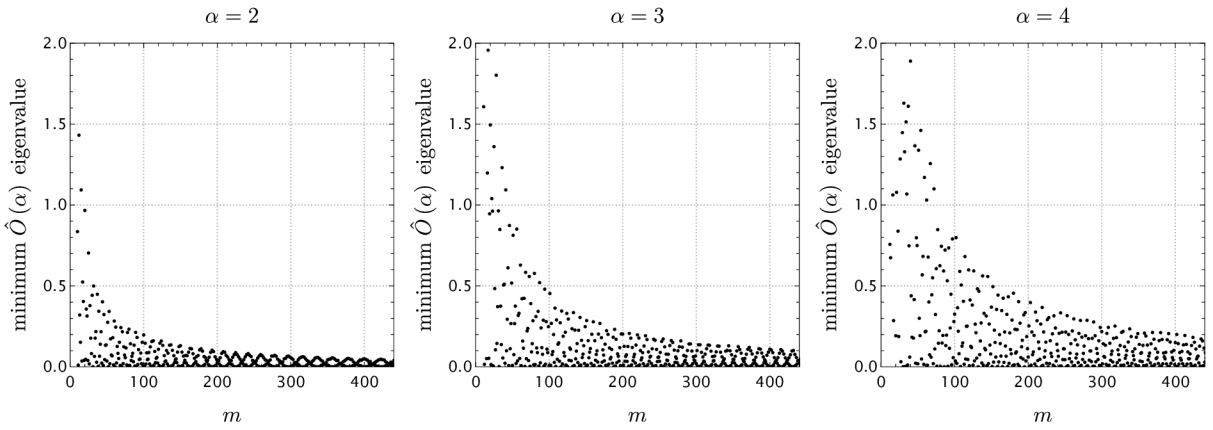

Figure 4.3: The dependence of minimum available eigenvalue of $\hat{O}(\alpha)$ on the truncated Fock space dimension m for $\alpha = 2, 3, 4$.

We know that the minimum eigenvalue for $m \to +\infty$ is zero and that there appears to be an upper bound in all plots. Within this bound, however, the behavior is quite chaotic due to truncated Fock space approximations. This does not mean that we cannot use the truncated operators for optimization. By construction, they should behave the way we expect the infinite-dimensional operator to, but we cannot make direct comparisons between Fock spaces of different dimensions.

In order to compare the behavior of $\hat{O}(\alpha)$ in truncated Fock spaces and in the infinite-dimensional Hilbert space a little more easily in the following work, we chose a dimension-displacement combination $m = 30, \alpha = 3.1$, because the finite-dimensional approximation of $\hat{O}(3.1)$ has (by chance) an extremely low ground state eigenvalue in the $30-$dimensional truncated Fock space. This does not imply that the expectation values of the approximated operator agree with the infinite-dimensional form in this case, but having similar minima allows us to easily scale them to compare their behavior.

4.2.2 Random gradient-like method

We have also developed a different method for finding the quantum state minimizing $\left\langle \hat{O}(\alpha) \right\rangle$. This method utilizes random kets to shift the states in a truncated Fock space closer to the optimal state. It can be described in the following simple steps:

0. choose a normalized starting state $|\text{temp}\rangle$,
1. generate a (pseudo)random normalized ket $|\text{shift}\rangle$,
2. evaluate $\left\langle \hat{O}(\alpha) \right\rangle$ for three states defined as

$$|-\rangle = \frac{|\text{temp}\rangle - \frac{1}{k}|\text{shift}\rangle}{\left\| |\text{temp}\rangle - \frac{1}{k}|\text{shift}\rangle \right\|}, \qquad |=\rangle = |\text{temp}\rangle, \qquad |+\rangle = \frac{|\text{temp}\rangle + \frac{1}{k}|\text{shift}\rangle}{\left\| |\text{temp}\rangle + \frac{1}{k}|\text{shift}\rangle \right\|}, \tag{4.2.1}$$

3. rename the state with smallest $\left\langle \hat{O}(\alpha) \right\rangle$ as $|\text{temp}\rangle$,
4. if $|\text{temp}\rangle$ did not change in a set amount of iterations, increase the precision value k,
5. repeat steps 1. to 4. until the optimization converges.

Its implementation in Python can be seen in A.3, both the need for precision increase and convergence are checked using counters. This method is based on the simple premise that unless you are standing sideways to your goal, you can always make some progress towards it by making a small enough step forwards or backwards. The journey may be treacherous, but you will eventually reach it (unless you stumble upon a local minimum).

In testing this method for $\left\langle \hat{O}(\alpha) \right\rangle$, we did not stumble upon any local minima, and it always converged to the eigenstate with the lowest eigenvalue for the given m and α, the same states which were found in the previous section. This is a good sign, but the true power of this method lies in the journey itself.

4.3 Embracing randomness

Using the random gradient-like optimization introduced in the previous section, we can actually compare the proposed evaluation methods for a plethora of states that would never explicitly come to mind. By choosing a random starting state every time, the optimization would eventually (after an infinite number of runs) go through all available states in the truncated Fock space. Given that it always converges to the same state, we can expect to get decent enough coverage for states similar to the optimal state after a finite number of runs. If we evaluate $\left\langle \hat{O}(\alpha) \right\rangle$ along with the interaction fidelities from section 3.1 for all $|\text{temp}\rangle$ states during each optimization run, we should obtain the best picture of which states actually behave like quadrature eigenket superpositions and which do not.

First, we need to generally implement the conditional measurements necessary for interaction-based evaluations, for which we can use the unitary descriptions in (3.1.2) and (3.1.11). Given the unitary transformation, we can find the conditional output in the second mode after measuring $p_1 = 0$ in the first mode as [32]

$$\hat{\rho}_{\text{COUT}_2} = \frac{\text{Tr}_1 \left[\hat{U}^\dagger \hat{\rho}_{\text{IN}_{12}} \hat{U} \left(|p_1 = 0\rangle_1 \langle p_1 = 0| \otimes \hat{\mathbb{1}}_2 \right) \right]}{\text{Tr} \left[\hat{U}^\dagger \hat{\rho}_{\text{IN}_{12}} \hat{U} \left(|p_1 = 0\rangle_1 \langle p_1 = 0| \otimes \hat{\mathbb{1}}_2 \right) \right]}, \tag{4.3.1}$$

where $\hat{\mathbb{1}}_2$ is the unitary operator of the second mode, $\hat{\rho}_{\text{IN}_{12}}$ is the joint input state before the unitary transformation $\hat{U}$, in our case (with pure states) $\hat{\rho}_{\text{IN}_{12}} = |\text{R}\rangle_1 \langle \text{R}| \otimes |0\rangle_2 \langle 0|$, and Tr_1 denotes the partial trace over the first subsystem [29].

The issue of obtaining $|p_1 = 0\rangle$ in a truncated Fock space was solved by approximating it by the most squeezed vacuum state, which is well approximated in the given space (per criterion (4.1.6)), similarly to section 1.2, only with squeezing in the orthogonal direction (to obtain an approximation of $|p = 0\rangle$ instead of $|x = 0\rangle$).

Over one hundred optimization runs from random starting states were performed for the aforementioned dimension-displacement combination $m = 30, \alpha = 3.1$ and a total of 1,090,137 unique quantum states were examined with $\left\langle \hat{O}(\alpha) \right\rangle$, F_{QND} and F_{BS} evaluated for all of them. F_{QND} denotes fidelity of the ideal QND output established in (3.1.5) and the output we obtain by using the examined state as the resource, F_{BS} denotes the same value for the beam splitter interaction. Results are plotted in figures 4.4, the code used can be viewed in A.4.

While it might seem that there is no connection between the fidelities and $\left\langle \hat{O}(\alpha) \right\rangle$, there is a very apparent lower bound starting at around $\left\langle \hat{O}(\alpha) \right\rangle = 0.15$ and states with lower expectation values only exhibit F_{QND} and F_{BS} above a certain boundary.

Careful examination of states which lie directly on this boundary (see figure 4.5) shows that these are states with minimized $\left\langle \hat{O}_1(\alpha) \right\rangle$, which differ only through values of $\left\langle \hat{O}_2(\alpha) \right\rangle$. This allows us to derive the boundary analytically, which is done in the next section.

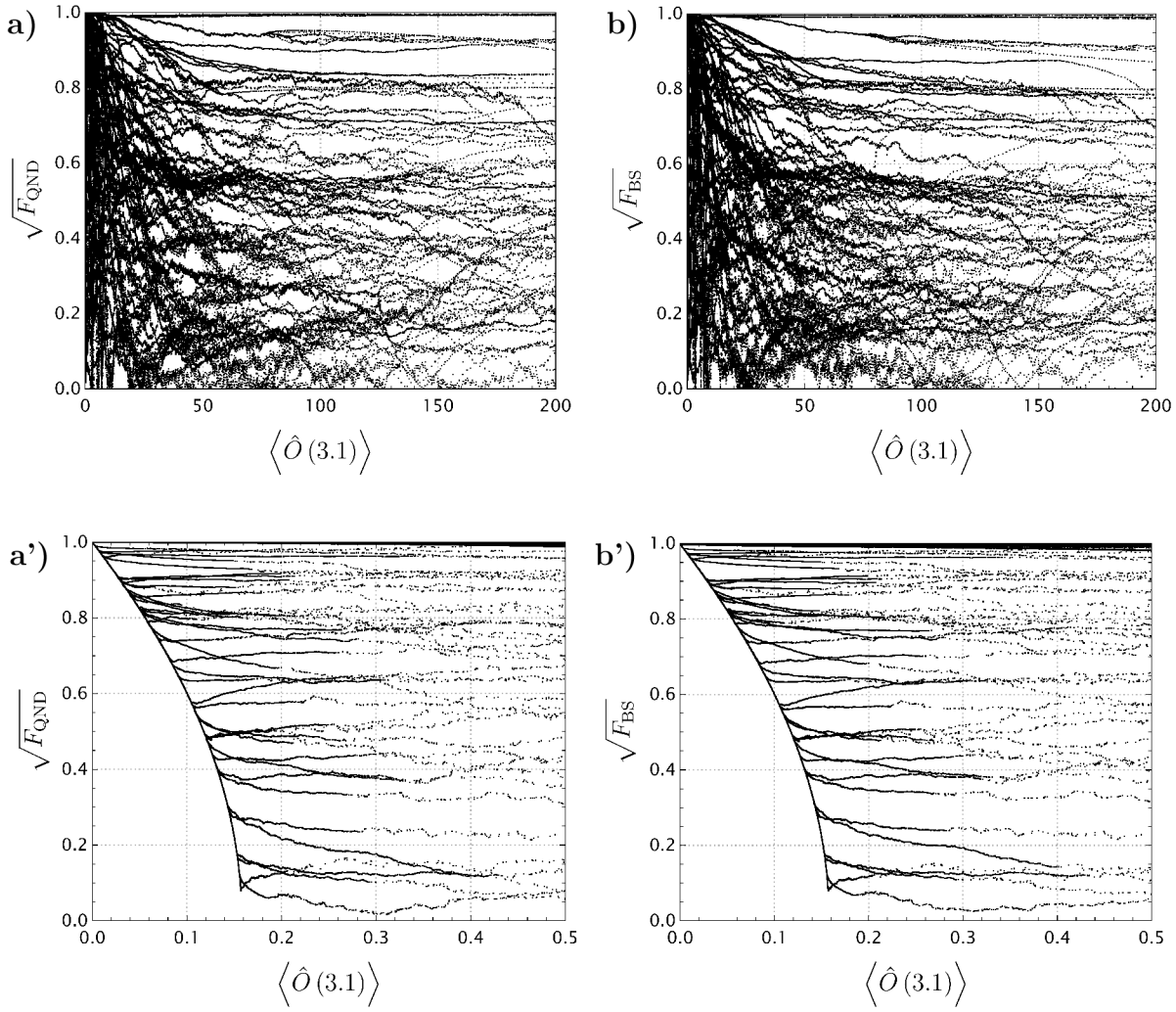

Figure 4.4: Results of the repeated random $\left\langle \hat{O}(\alpha) \right\rangle$ minimization for $m = 30, \alpha = 3.1$ with plots of **a)** $\sqrt{F_{\mathrm{QND}}}$ and **b)** $\sqrt{F_{\mathrm{BS}}}$.[a] The primed plots are zoomed-in leftmost sections of the non-primed plots. The individual optimization runs are clearly visible in the zoomed-in plots as well as a boundary curve, left of which no quantum states were found.

[a] The `QuTiP` library defines fidelity according to [1], which corresponds to the square root of our fidelity.

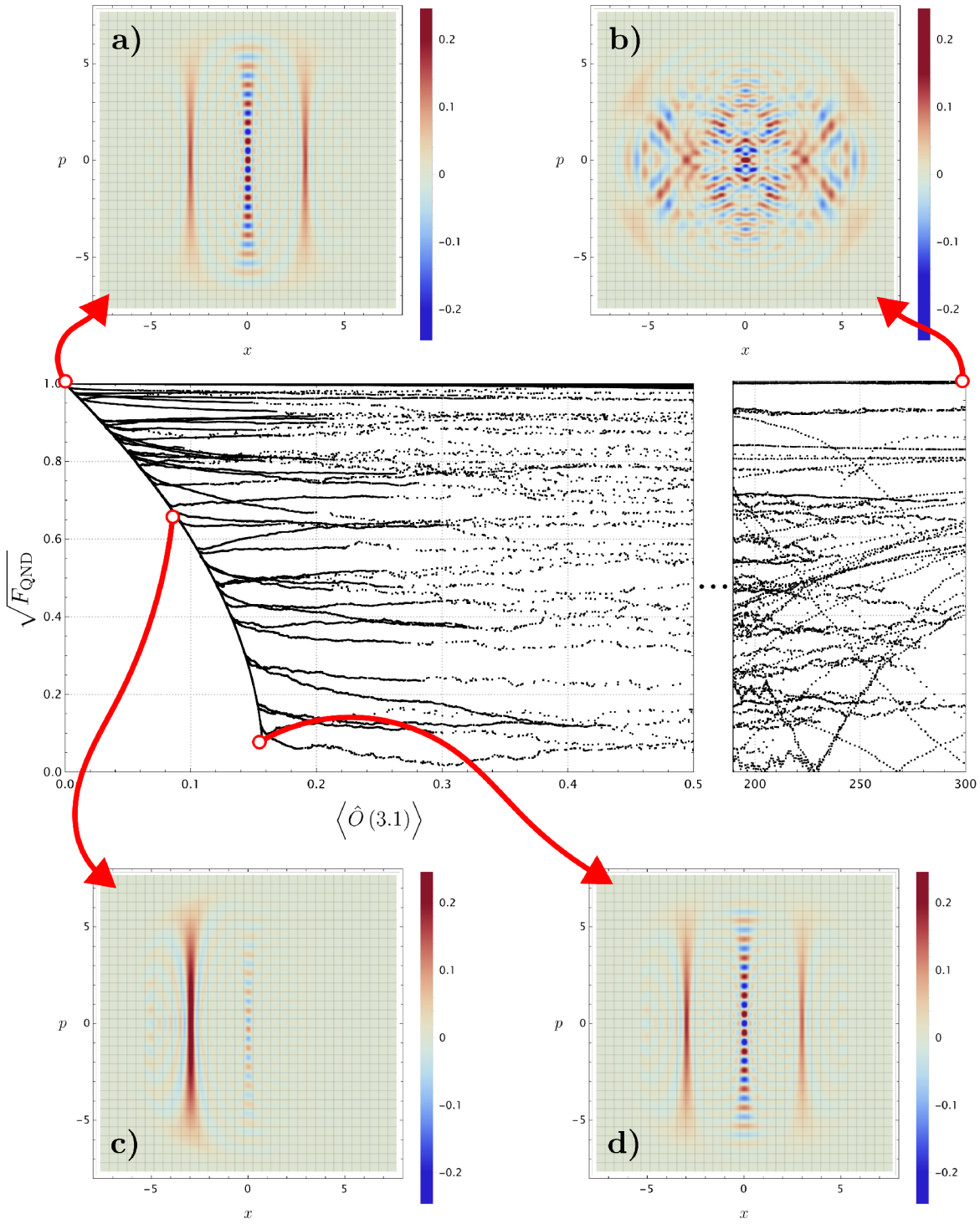

Figure 4.5: Results of the repeated random $\left\langle \hat{O}(\alpha) \right\rangle$ minimization for $m = 30, \alpha = 3.1$ with highlighted important states: **a)** the optimal (even) squeezed cat state, **b)** a new catlike state, **c)** a squeezed displaced state, **d)** the odd squeezed cat state.

4.3.1 Finding boundaries

We postulate that in the Hilbert space spanned by $\hat{x}$ and $\hat{p}$, all pure states minimizing $\left\langle \hat{O}_1(\alpha) \right\rangle$ (i.e. the boundary states) are superpositions of the form

$$|\xi_{\alpha,\infty,w}\rangle = w\,|\alpha\rangle + |-\alpha\rangle\,, \tag{4.3.2}$$

where $w \in \mathbb{R}$. This state can be thought of as the large squeezing limit of

$$|\xi_{\alpha,r,w}\rangle = \frac{1}{N_{\alpha,r,w}}\left(w\hat{D}_x(\alpha)\hat{S}(r)\,|0\rangle + \hat{D}_x(-\alpha)\hat{S}(r)\,|0\rangle\right), \tag{4.3.3}$$

The $x-$representation wave function of this state is

$$\langle x|\xi_{\alpha,r,w}\rangle = \frac{e^{-\frac{e^{2r}(x+\alpha)^2}{2}} + we^{-\frac{e^{2r}(x-\alpha)^2}{2}}}{\sqrt{\sqrt{\pi}\,e^{-r}w^2 + 2\sqrt{\pi}\,e^{-\alpha^2e^{2r}-r}w + \sqrt{\pi}\,e^{-r}}} \tag{4.3.4}$$

and the $p-$representation is therefore

$$\langle p|\xi_{\alpha,r,w}\rangle = \frac{e^{\frac{e^{-2r}\left(-p^2+\alpha^2e^{4r}-re^{2r}\right)}{2}}\left((w+1)\cos(\alpha p) - i\,(w-1)\sin(\alpha p)\right)}{\sqrt[4]{\pi}\sqrt{w\left(e^{\alpha^2e^{2r}}w+2\right)+e^{\alpha^2e^{2r}}}}. \tag{4.3.5}$$

We can explicitly evaluate the expectation value of $\hat{O}_2(\alpha)$ for this state as

$$\left\langle \hat{O}_2(\alpha)\right\rangle_{\xi_{\alpha,r,w}} = \frac{(w-1)^2\exp\left[\alpha^2e^{2r} - \frac{e^{-2r}\pi^2}{4\alpha^2} - r\right]}{\left[\exp\left(-\frac{e^{-2r}\pi^2}{\alpha^2}\right)\right]^{\frac{1}{4}}\sqrt{\pi}\left[2w + \exp\left(\alpha^2e^{2r}\right)(1+w^2)\right]}\,\vartheta_2\left[\exp\left(-\frac{\pi^2}{\alpha^2e^{2r}}\right)\right], \tag{4.3.6}$$

where $\vartheta_2[q] = 2q^{1/4}\sum_{n=0}^{+\infty}q^{n(n+1)}$ is the second elliptic theta constant. Using equations (3.1.7) and (3.1.14) we can also straightforwardly calculate the conditional outputs in the QND interaction and the beam splitter as

$$\langle x_2|\text{QND\_COUT}\rangle_{\xi_{\alpha,r,w}} = \frac{\left(we^{\frac{2\alpha e^{2r}x_2}{e^{2r}+1}}+1\right)e^{-\frac{e^{2r}x_2^2+2\alpha e^{2r}x_2-re^{2r}-r}{2\left(e^{2r}+1\right)}}}{\sqrt[4]{\pi}\sqrt[4]{e^{2r}+1}\sqrt{w\left(e^{\alpha^2e^{2r}}w+2\right)+e^{\alpha^2e^{2r}}}\sqrt{\frac{w\left(e^{\frac{\alpha^2e^{2r}}{e^{2r}+1}}w+2\right)+e^{\frac{\alpha^2e^{2r}}{e^{2r}+1}}}{w\left(e^{\alpha^2e^{2r}}w+2\right)+e^{\alpha^2e^{2r}}}}}, \tag{4.3.7}$$

$$\langle x_2|\text{BS\_COUT}\rangle_{\xi_{\alpha,r,w}} = \frac{\left(we^{\frac{\sqrt{2}\,\alpha e^{4r}x_2}{e^{2r}+1}}+e^{\frac{\sqrt{2}\,\alpha e^{2r}\left(e^{2r}+2\right)x_2}{e^{2r}+1}}\right)e^{-\frac{2^{\frac{5}{2}}e^{2r}x_2^2+8\alpha e^{4r}x_2+8\alpha e^{2r}x_2-2^{\frac{3}{2}}re^{2r}-2^{\frac{3}{2}}r}{2^{\frac{5}{2}}\left(e^{2r}+1\right)}}}{\sqrt[4]{\frac{\pi}{2}}\sqrt[4]{e^{2r}+1}\sqrt{w\left(e^{\alpha^2e^{2r}}w+2\right)+e^{\alpha^2e^{2r}}}\sqrt{\frac{w\left(e^{\frac{\alpha^2e^{2r}}{e^{2r}+1}}w+2\right)+e^{\frac{\alpha^2e^{2r}}{e^{2r}+1}}}{w\left(e^{\alpha^2e^{2r}}w+2\right)+e^{\alpha^2e^{2r}}}}} \tag{4.3.8}$$

and the fidelities with optimal outputs as

$$F = F_{\mathrm{QND}} = F_{\mathrm{BS}} = \frac{e^r\sqrt{e^{2r}+1}\left(e^{\frac{\alpha^2}{2\left(e^{2r}+1\right)\left(2e^{2r}+1\right)}}+e^{\frac{\alpha^2\left(2e^{2r}+1\right)}{2\left(e^{2r}+1\right)}}\right)^2(w+1)^2}{\left(e^{\alpha^2}+1\right)\left(2e^{2r}+1\right)\left(w\left(e^{\frac{\alpha^2e^{2r}}{e^{2r}+1}}w+2\right)+e^{\frac{\alpha^2e^{2r}}{e^{2r}+1}}\right)}. \tag{4.3.9}$$

It is clear that $F_{\mathrm{BS}} = F_{\mathrm{QND}} = 0$ for an odd squeezed cat state with $w = -1$ and that these expressions convert to ones we obtained before for the original case with $w = 1$. Even and odd eigenket superpositions thus give oppositely correlated, orthogonal results in these interactions. Equation (4.3.9) also implies that the boundary is identical for both F_{BS} and F_{QND}.

We can now compare equations (4.3.6) and (4.3.9) to eliminate w and then solve for F in the limit of large squeezing to obtain

$$F_{\min}\left(\alpha,\left\langle\hat{O}(\alpha)\right\rangle\right) = \begin{cases} 1-\dfrac{\sqrt{\pi}\left\langle\hat{O}(\alpha)\right\rangle}{2\vartheta_2\left[\exp\left(-\frac{\pi^2}{\alpha^2}\right)\right]}, & \text{for } \left\langle\hat{O}(\alpha)\right\rangle \in \left[0,\dfrac{2\vartheta_2\left[\exp\left(-\frac{\pi^2}{\alpha^2}\right)\right]}{\sqrt{\pi}}\right] \\ 0, & \text{otherwise,} \end{cases}, \tag{4.3.10}$$

where we used the fact that $\left\langle\hat{O}_2(\alpha)\right\rangle \to \left\langle\hat{O}(\alpha)\right\rangle$ as $r \to +\infty$ for all w. Equation (4.3.10) was obtained for $e^{-\alpha^2} \ll 1$ and is therefore only an approximation that works extremely well for $\alpha \gtrapprox 2$ (maximum error of $\delta F_{\min} \doteq 0.002$ for $\alpha = 2.5$). For smaller α, the exact form is

$$F_{\min}\left(\alpha,\left\langle\hat{O}(\alpha)\right\rangle\right) = \lim_{r\to+\infty}\frac{\left(e^{\alpha^2}+1\right)\left[\sqrt{\pi}e^r\left(1-e^{\alpha^2e^{2r}}\right)\left\langle\hat{O}(a)\right\rangle+2e^{\alpha^2e^{2r}}\vartheta_2\left[\exp\left(-\frac{\pi^2}{\alpha^2e^{2r}}\right)\right]\right]}{2\sqrt{\pi}e^r\left(e^{\alpha^2}-e^{\alpha^2e^{2r}}\right)\left\langle\hat{O}(\alpha)\right\rangle+2e^{\alpha^2e^{2r}}\left(e^{\alpha^2}+1\right)\vartheta_2\left[\exp\left(-\frac{\pi^2}{\alpha^2e^{2r}}\right)\right]}. \tag{4.3.11}$$

Using the explicit boundary curve equation, we can now visualize the relationship between QND/BS output fidelity and $\left\langle\hat{O}\left(\alpha\right)\right\rangle$ for any set displacement in an infinite-dimensional Hilbert space, see figure 4.6.

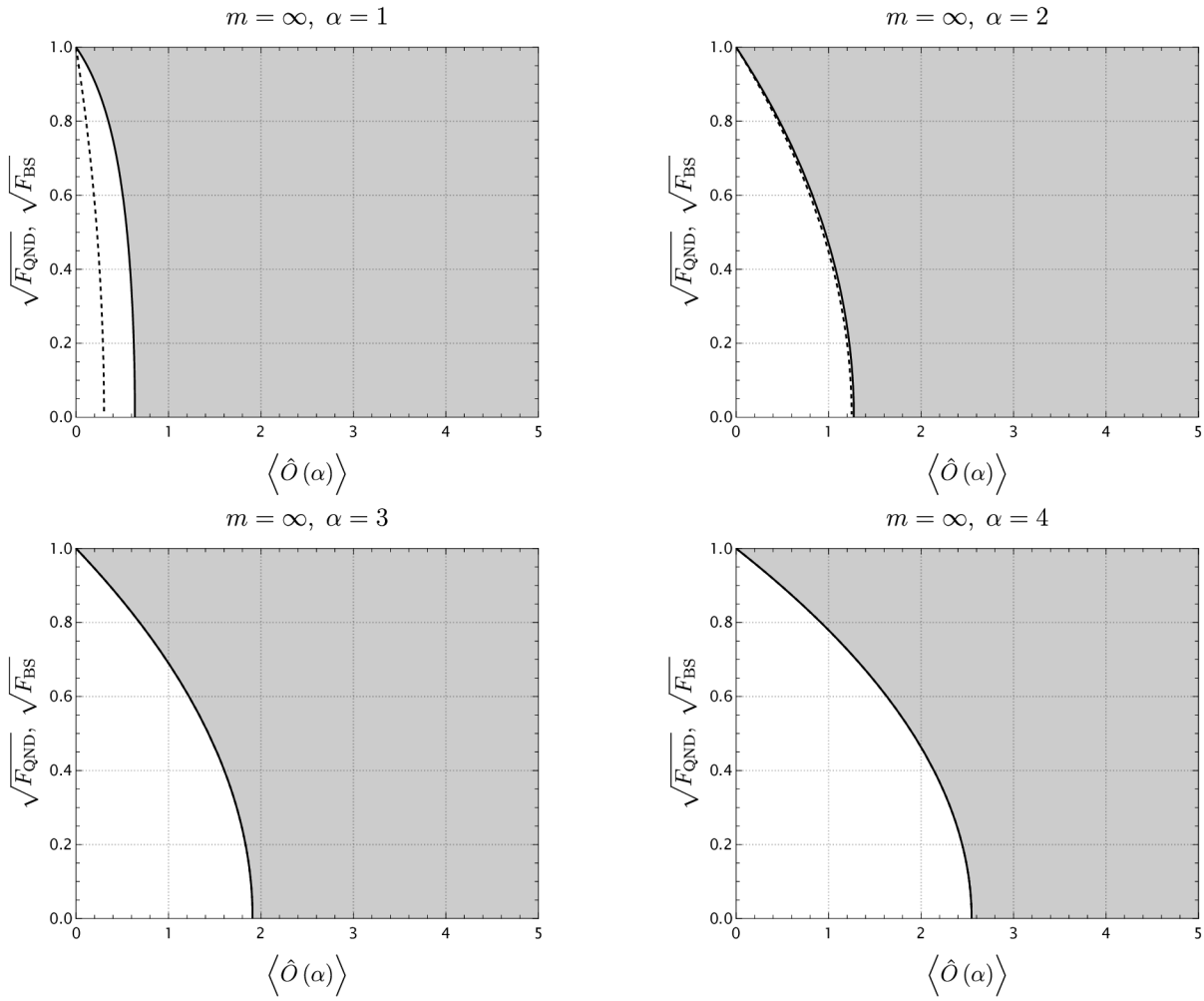

Figure 4.6: Analytical relations between $\left\langle \hat{O}(\alpha) \right\rangle$ and possible $\sqrt{F_{\mathrm{QND}}}, \sqrt{F_{\mathrm{BS}}}$ for various values of α, gray filling signifies the existence of quantum states with specific $\sqrt{F}$ and $\left\langle \hat{O}(\alpha) \right\rangle$. Dashed lines correspond to (4.3.10) and full lines were found using (4.3.11), they overlap perfectly in the bottom two plots.

It is apparent that the simplified form (4.3.10) works well for sufficiently large values of α and we can also see that the boundary behaves very similarly to the one found through numerical optimization, even though the values of $\left\langle \hat{O}(\alpha) \right\rangle$ do not align.

This can be attributed partly to the fact that we have chosen a very optimistic combination of m, α for the optimization, where the optimal state returns $\left\langle \hat{O}(3.1) \right\rangle = 2.39 \cdot 10^{-6}$, even though evaluating it in an infinite-dimensional space returns larger values. This is caused by using a truncated Fock basis form of $\hat{O}(\alpha)$, but let us not forget that we have also used the harmonic approximation of $\hat{O}_2(\alpha)$ from equation (3.2.3), which is not normalized in the same way as the original form of the operator from equation (3.2.2). This is most likely the main cause of the shift in values. We can compare the analytical boundary with the one found numerically by scaling it appropriately, see figure 4.7.

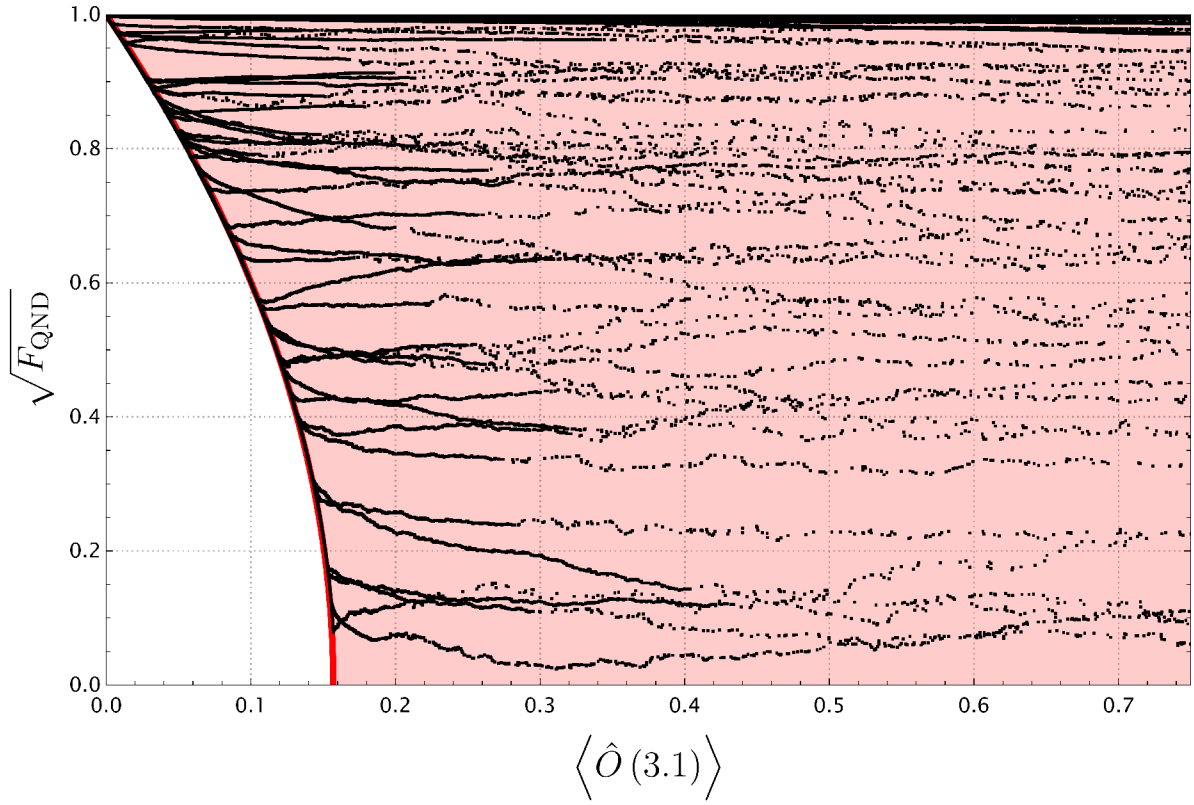

Figure 4.7: Comparison between numerical data and the analytical relation between $\left\langle \hat{O}(\alpha) \right\rangle$ and possible $\sqrt{F_{\mathrm{QND}}}$. The thick red line was found using (4.3.10) with a scaling factor of 12.57 in the argument.

The appropriately scaled analytical boundary agrees with the numerical optimization data almost perfectly. This suggests that we have found the correct relationship analytically and that the truncated Fock basis numerical optimization does actually give data which agrees with the infinite-dimensional case, just scaled differently because of the $\hat{O}_2(\alpha)$ approximation employed.

Note that we can shift the boundary to the right by giving $\hat{O}_2(\alpha)$ a larger weight in (3.2.4) and also note that the existence of quantum states in the entire filled area is only postulated; we have not established whether any bounds for large $\left\langle \hat{O}(\alpha) \right\rangle$ exist.

4.3.2 New cat-like states

We have also found states that exhibit large values of $\left\langle \hat{O}(\alpha) \right\rangle$, while still achieving very high fidelity outputs. Two of these states are visualized in figures 4.8 and 4.9 along with their respective QND and BS outputs. The same is done for the optimal state in figure 4.10.

We can see that both of the new states create outputs with very high fidelities in the QND interaction; however, the second state performs quite poorly in terms of beam splitter fidelity. We have already mentioned that F_{QND} and F_{BS} do not necessarily have to be the same for general states and it is apparent that these two values can differ significantly. Both of the new states only contain real coefficients, which are non zero only for even-numbered Fock states, similarly to squeezed cat states; however, the coefficient structure is very different.

A big challenge is to replicate states from figures 4.8 and 4.9 analytically in an infinite-dimensional Hilbert space and potentially find more states which behave this way. One good question to ask is whether an upper bound for the fidelities exists based on $\left\langle \hat{O}(\alpha) \right\rangle$. We had already established that the expectation value is unbounded; therefore, there may not be an upper fidelity bound at all, but this is only the case for an infinite-dimensional space, which also suggests that numerical analysis in truncated Fock spaces will not help us in finding an upper bound.

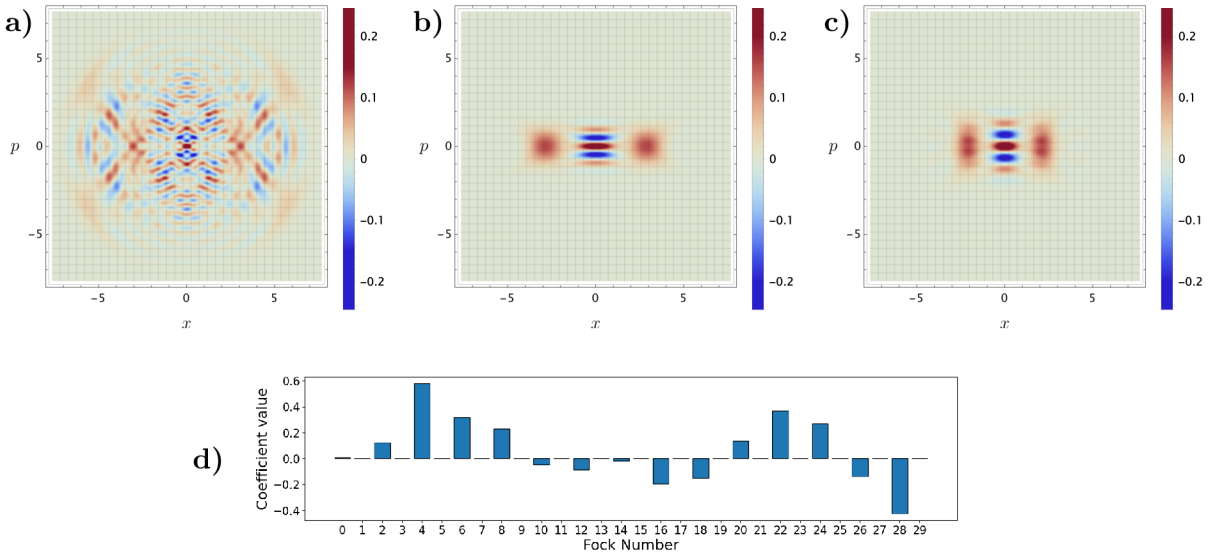

Figure 4.8: **a)** New cat-like state Wigner function along with conditional outputs in **b)** the QND interaction and **c)** the beam splitter. Fock coefficients of the top left state are shown in **d)**, this state achieves $F_{\mathrm{QND}} = 0.992, F_{\mathrm{BS}} = 0.996$ with $\left\langle \hat{O}(\alpha) \right\rangle = 291$ for $\alpha = 3.1$.

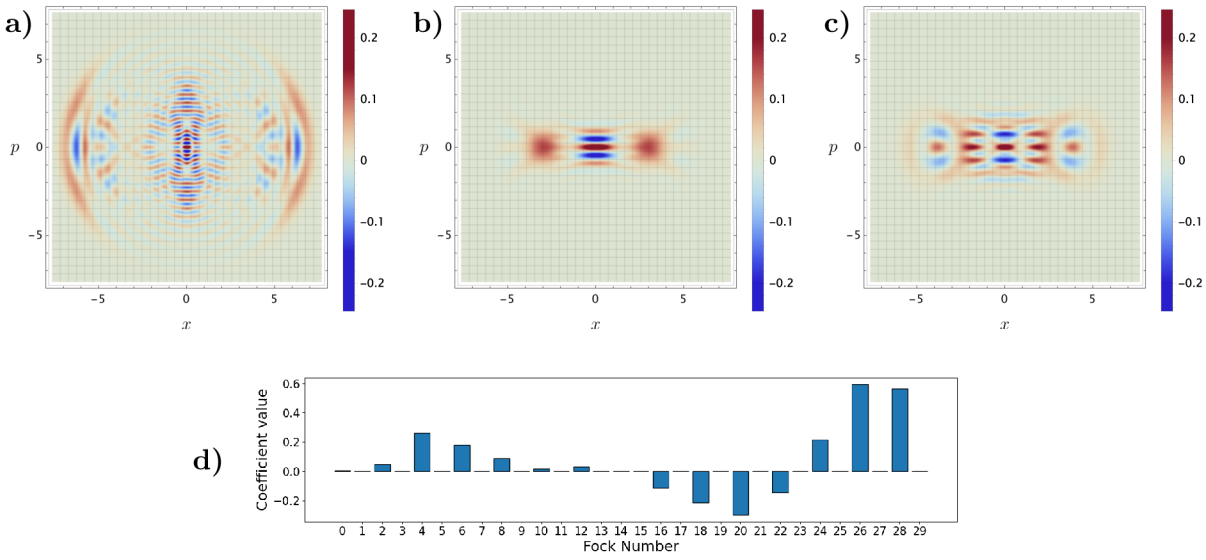

Figure 4.9: **a)** New cat-like state Wigner function along with conditional outputs in **b)** the QND interaction and **c)** the beam splitter. Fock coefficients of the top left state are shown in **d)**, this state achieves $F_{\mathrm{QND}} = 0.990, F_{\mathrm{BS}} = 0.732$ with $\left\langle \hat{O}(\alpha) \right\rangle = 957$ for $\alpha = 3.1$.

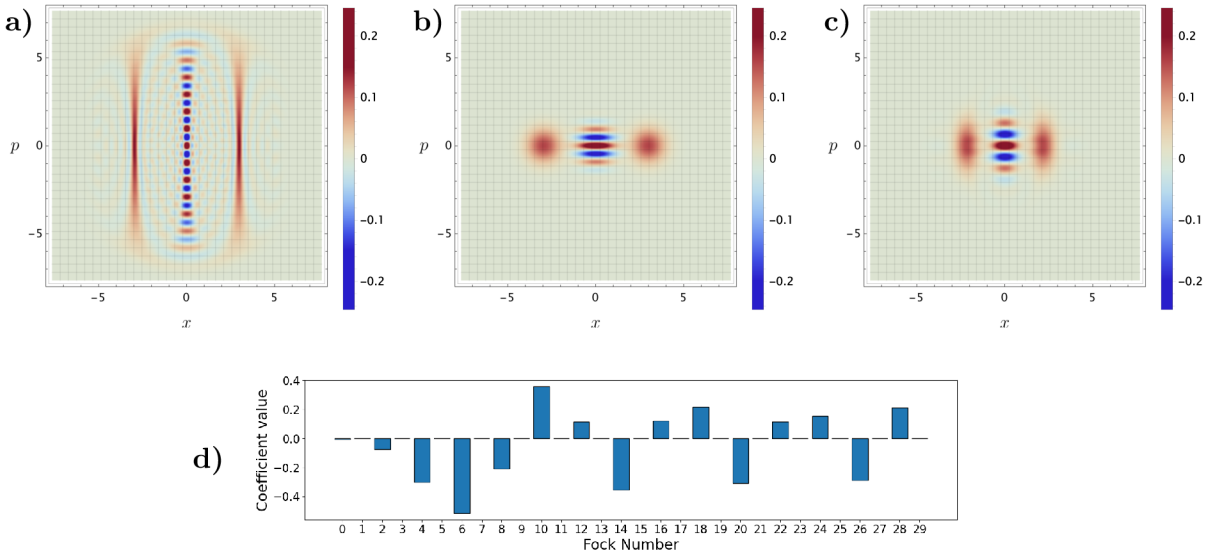

Figure 4.10: **a)** The optimal state Wigner function along with conditional outputs in **b)** the QND interaction and **c)** the beam splitter. Fock coefficients of the top left state are shown in **d)**, this state achieves $F_{\mathrm{QND}} = 0.999, F_{\mathrm{BS}} = 0.996$ with $\left\langle \hat{O}(\alpha) \right\rangle = 2.39 \cdot 10^{-6}$ for $\alpha = 3.1$.

Conclusions

Throughout this thesis, the widely established theoretical framework of quantum optics was employed to examine the properties of even quadrature eigenket superpositions and subsequently devise methods to evaluate their approximations. In the first chapter, we have reached the conclusions that quadrature eigenkets can be thought of as the large squeezing limits of squeezed displaced states and that highly squeezed states therefore function as their approximations. We have also explicitly shown that quantum state fidelity gives us minimal information about how well a certain state approximates a quadrature eigenket, due to insufficient connection between fidelity and the quadrature variance ratio of two states.

The remainder of this work was focused on even superpositions of oppositely displaced quadrature eigenkets and their approximations. After a short examination of the various representations and properties of squeezed cat states, which again converge to the desired eigenket superpositions in the limit of large squeezing, two interaction-based evaluation methods were described. We have shown that by using a squeezed cat state as the resource for an interaction with the vacuum state in a beam splitter or a quantum nondemolition interaction, we can draw conclusions about the squeezing of constituent states by evaluating the fidelity of the obtained output with the ideal output state, which would have been expected if we had used the eigenket superposition instead.

The main result of this work is the construction of a new operator $\hat{O}(\alpha)$, based entirely on the properties of even eigenket superpositions. We have initially shown that for squeezed cat states, its expectation value is minimized at zero for a superposition of infinitely squeezed states at $x = \pm\alpha$ and then we have also shortly examined how this operator detects decoherence of squeezed cat states.

To establish the usefulness of this operator, numerical optimization with random starting points was performed in a truncated Fock space, which allowed us to compare the expectation value of $\hat{O}(\alpha)$ along with the aforementioned beam splitter and QND fidelities. Using the results of this optimization, we analytically derived a parametric boundary that allows us to set a lower bound for the ideal output fidelity in both interactions simply by finding the operator expectation value. This suggests that the presented evaluation methods agree with each other, that the even eigenket superposition can be found by minimizing $\hat{O}(\alpha)$, and that predictions about the interaction fidelities can be made solely based on its expectation value.

Outlook

Many stones were left unturned by this thesis. It has not been determined whether there is a way to directly measure $\hat{O}(\alpha)$ or any of its approximations. As a hermitian operator, it represents an observable in theory, but no experimental schemes were discussed. Regarding the operator itself, the generalization to an odd eigenket superposition and superpositions with a general phase difference between constituent states remains an open question, along with the optimal weights assigned to operators $\hat{O}_1(\alpha)$ and $\hat{O}_2(\alpha)$. The generalization of $\hat{O}(\alpha)$ should be achievable simply by displacing the projection eigenkets in $\hat{O}_2(\alpha)$ to match up with zeros of the $p-$probability distribution of the general superposition, whereas the question of optimal weighting will most probably have multiple application-dependent solutions.

We have also mentioned that one of the primary uses for eigenket superposition approximations is the preparation of GKP states, and it would also be reasonable to explore how the expectation values of $\hat{O}(\alpha)$ for resource states in breeding protocols influence the obtained grid states. In order to simplify the answer to this question, a similar operator-based evaluation method for GKP states could also be developed – this can probably be achieved for any of the states mentioned in [2].

Methods

Wolfram Engine 13.1 [33] was used to perform algebraic simplification, evaluate infinite sums, create graphics and evaluate definite integrals. Maxima was used to evaluate some definite integrals. Python 3.10.11 [34] with the `QuTiP` [31] and `NumPy` [35] libraries was used for numerical calculations in truncated Fock spaces. Typeset using XeLaTeX with BibTeX.

Bibliography

Books

[1] Nielsen, M. A. and Chuang, I. L. *Quantum Computation and Quantum Information*. en. Cambridge, England: Cambridge University Press, June 2012.

[10] Leonhardt, U. *Measuring the quantum state of light*. en. Cambridge studies in modern optics. Cambridge, England: Cambridge University Press, July 1997.

[11] Sakurai, J. J. and Napolitano, J. J. *Modern Quantum Mechanics: Pearson New International Edition*. en. 2nd ed. London, England: Pearson Education, July 2013.

[13] Walls, D. F. and Milburn, G. J. *Quantum Optics*. en. Springer Study Edition. Berlin, Germany: Springer, Apr. 1994.

[29] Peres, A. *Quantum Theory: Concepts and Methods*. en. Fundamental Theories of Physics. Dordrecht, Netherlands: Springer, Oct. 1993.

Online resources

[2] Joshi, A., Noh, K., and Gao, Y. Y. "Quantum information processing with bosonic qubits in circuit QED." In: *Quantum Science and Technology* 6.3 (Apr. 2021), p. 033001. URL: https://doi.org/10.1088/2058-9565/abe989.

[3] Steane, A. M. "Error Correcting Codes in Quantum Theory." In: *Physical Review Letters* 77.5 (July 1996), pp. 793–797. URL: https://doi.org/10.1103/physrevlett.77.793.

[4] Schlegel, D. S., Minganti, F., and Savona, V. "Quantum error correction using squeezed Schrödinger cat states." In: *Physical Review A* 106.2 (Aug. 2022). URL: https://doi.org/10.1103/physreva.106.022431.

[5] Weigand, D. J. and Terhal, B. M. "Generating grid states from Schrödinger-cat states without postselection." In: *Phys. Rev. A (Coll. Park.)* 97.2 (Feb. 2018).

[6] Gottesman, D., Kitaev, A., and Preskill, J. "Encoding a qubit in an oscillator." In: *Physical Review A* 64.1 (June 2001). URL: https://doi.org/10.1103/physreva.64.012310.

[7] Vasconcelos, H. M., Sanz, L., and Glancy, S. "All-optical generation of states for "Encoding a qubit in an oscillator"." In: *Optics Letters* 35.19 (Sept. 2010), p. 3261. URL: https://doi.org/10.1364/ol.35.003261.

[8] Huang, K., Jeannic, H. L., Ruaudel, J., Verma, V., Shaw, M., Marsili, F., Nam, S., Wu, E., Zeng, H., Jeong, Y.-C., Filip, R., Morin, O., and Laurat, J. "Optical Synthesis of Large-Amplitude Squeezed Coherent-State Superpositions with Minimal Resources." In: *Physical*

Review Letters 115.2 (July 2015). URL: https://doi.org/10.1103/physrevlett.115.023602.

[9] Hastrup, J. and Andersen, U. L. "Protocol for Generating Optical Gottesman-Kitaev-Preskill States with Cavity QED." In: *Physical Review Letters* 128.17 (Apr. 2022). URL: https://doi.org/10.1103/physrevlett.128.170503.

[12] Madrid, R. de la. "The role of the rigged Hilbert space in quantum mechanics." In: *European Journal of Physics* 26.2 (Feb. 2005), pp. 287–312. URL: https://doi.org/10.1088/0143-0807/26/2/008.

[14] Munguía-González, E., Rego, S., and Freericks, J. K. "Making squeezed-coherent states concrete by determining their wavefunction." In: *American Journal of Physics* 89.9 (Sept. 2021), pp. 885–896. URL: https://doi.org/10.1119/10.0004872.

[15] Jozsa, R. "Fidelity for Mixed Quantum States." In: *Journal of Modern Optics* 41.12 (Dec. 1994), pp. 2315–2323. URL: https://doi.org/10.1080/09500349414552171.

[16] Tse, M. et al. "Quantum-Enhanced Advanced LIGO Detectors in the Era of Gravitational-Wave Astronomy." In: *Physical Review Letters* 123.23 (Dec. 2019). URL: https://doi.org/10.1103/physrevlett.123.231107.

[17] Serafini, A., Siena, S. D., Illuminati, F., and Paris, M. G. A. "Minimum decoherence cat-like states in Gaussian noisy channels." In: *Journal of Optics B: Quantum and Semiclassical Optics* 6.6 (May 2004), S591–S596. URL: https://doi.org/10.1088/1464-4266/6/6/019.

[18] Jeong, H. and Kim, M. S. "Efficient quantum computation using coherent states." In: *Physical Review A* 65.4 (Mar. 2002). URL: https://doi.org/10.1103/physreva.65.042305.

[19] Ralph, T. C., Gilchrist, A., Milburn, G. J., Munro, W. J., and Glancy, S. "Quantum computation with optical coherent states." In: *Physical Review A* 68.4 (Oct. 2003). URL: https://doi.org/10.1103/physreva.68.042319.

[20] Dakna, M., Anhut, T., Opatrný, T., Knöll, L., and Welsch, D.-G. "Generating Schrödinger-cat-like states by means of conditional measurements on a beam splitter." In: *Physical Review A* 55.4 (Apr. 1997), pp. 3184–3194. URL: https://doi.org/10.1103/physreva.55.3184.

[21] Walshe, B. W., Baragiola, B. Q., Alexander, R. N., and Menicucci, N. C. "Continuous-variable gate teleportation and bosonic-code error correction." In: *Physical Review A* 102.6 (Dec. 2020). URL: https://doi.org/10.1103/physreva.102.062411.

[22] Farley, A. and D'Eath, P. "Coherent and squeezed states in black-hole evaporation." In: *Physics Letters B* 634.4 (Mar. 2006), pp. 419–426. URL: https://doi.org/10.1016/j.physletb.2006.01.020.

[23] Kamra, A., Thingstad, E., Rastelli, G., Duine, R. A., Brataas, A., Belzig, W., and Sudbø, A. "Antiferromagnetic magnons as highly squeezed Fock states underlying quantum correlations." In: *Physical Review B* 100.17 (Nov. 2019). URL: https://doi.org/10.1103/physrevb.100.174407.

[24] Parikh, M., Wilczek, F., and Zahariade, G. "Signatures of the quantization of gravity at gravitational wave detectors." In: *Physical Review D* 104.4 (Aug. 2021). URL: https://doi.org/10.1103/physrevd.104.046021.

[25] López-Díaz, M., Sordo, M. A., and Suárez-Llorens, A. "On the L_p-metric between a probability distribution and its distortion." In: *Insurance: Mathematics and Economics* 51.2 (Sept. 2012), pp. 257–264. URL: https://doi.org/10.1016/j.insmatheco.2012.04.004.

[26] Brogaard, J. "Wigner function formalism in Quantum mechanics." Bachelor's Thesis. Copenhagen, Denmark: University of Copenhagen, June 2015. URL: https://nbi.ku.dk/english/theses/bachelor-theses/jon-brogaard/Jon_Brogaard_Bachelorthesis_2015.pdf.

[27] Filip, R., Marek, P., and Andersen, U. L. "Measurement-induced continuous-variable quantum interactions." In: *Physical Review A* 71.4 (Apr. 2005). URL: https://doi.org/10.1103/physreva.71.042308.

[28] Yoshikawa, J.-i., Miwa, Y., Huck, A., Andersen, U. L., Loock, P. van, and Furusawa, A. "Demonstration of a Quantum Nondemolition Sum Gate." In: *Physical Review Letters* 101.25 (Dec. 2008). URL: https://doi.org/10.1103/physrevlett.101.250501.

[30] Provazník, J., Filip, R., and Marek, P. "Taming numerical errors in simulations of continuous variable non-Gaussian state preparation." In: *Scientific Reports* 12.1 (Oct. 2022). URL: https://doi.org/10.1038/s41598-022-19506-9.

[31] Johansson, J., Nation, P., and Nori, F. "QuTiP 2: A Python framework for the dynamics of open quantum systems." In: *Computer Physics Communications* 184.4 (Apr. 2013), pp. 1234–1240. URL: https://doi.org/10.1016/j.cpc.2012.11.019.

[32] Ban, M. "Photon statistics of conditional output states of lossless beam splitter." In: *Journal of Modern Optics* 43.6 (June 1996), pp. 1281–1303. URL: https://doi.org/10.1080/09500349608232803.

[33] Wolfram Research, Inc. *Mathematica Language, Version 13.1*. Champaign, IL, 2022. URL: https://www.wolfram.com/mathematica.

[34] Van Rossum, G. and Drake, F. L. *Python 3 Reference Manual*. Scotts Valley, CA, 2009. URL: https://docs.python.org/3/reference/index.html.

[35] Harris, C. R., Millman, K. J., Walt, S. J. van der, Gommers, R., Virtanen, P., Cournapeau, D., Wieser, E., Taylor, J., Berg, S., Smith, N. J., Kern, R., Picus, M., Hoyer, S., Kerkwijk, M. H. van, Brett, M., Haldane, A., Río, J. F. del, Wiebe, M., Peterson, P., Gérard-Marchant, P., Sheppard, K., Reddy, T., Weckesser, W., Abbasi, H., Gohlke, C., and Oliphant, T. E. "Array programming with NumPy." In: *Nature* 585.7825 (Sept. 2020), pp. 357–362. URL: https://doi.org/10.1038/s41586-020-2649-2.

Appendix A

Code examples

A.1 Finding minimum eigenvalue eigenkets

```
from qutip import *
import numpy as np
import csv

def find_minimum_eigenvalue_vector(operator):

  eigvals, eigstates = operator.eigenstates()
  ground_eigvalue = eigvals[0]
  ground_state = eigstates[0]

  return ground_eigvalue, ground_state
```

This function returns a tuple containing the minimum eigenvalue and its associated eigenstate of `operator`, which is assumed to have only non-negative real eigenvalues. Note that it is necessary to include "`Sparse=True`" in the `eigenstates` function options for large truncated Fock space dimensions because of memory constraints. This snippet also contains the necessary imports for all code in this appendix.

A.2 Finding the best well approximated states

The following code defines a function, which returns the most squeezed cat state with displacement a, that is well approximated in the $N-$dimensional Fock space, and a function that returns the best approximation for the $|p = 0\rangle$ eigenket in the same space, which is then used to define the measurement projector in A.4.

```
def squeezed_cat(N,a,r):

  plus = displace(N,a/np.sqrt(2))*squeeze(N,r)*basis(N,0)
  minus = displace(N,-a/np.sqrt(2))*squeeze(N,r)*basis(N,0)

  return (plus+minus).unit()

def find_maximum_squeezing_cat(N,a):

  r = 0
  well_approximated = True

  while well_approximated:
    test_state = squeezed_cat(N*10,a,r)
    coefs = test_state.data.toarray().flatten()
    probability = 0

    for i in range(N):
      probability += coefs[i]**2

    if probability < 0.99:
      well_approximated = False
    else:
      r += 0.01

  return squeezed_cat(N,a,r-0.01)

def find_optimal_p0(N):

  r = -1
  well_approximated = True

  while well_approximated:
    test_state = squeeze(10*N,r)*basis(10*N,0)
    coefs = test_state.data.toarray().flatten()
    probability = 0

    for i in range(N):
      probability += coefs[i]**2

    if probability < 0.99:
      well_approximated = False
    else:
      r -= 0.01

  return squeeze(N,r+0.01)*basis(N,0)

```

A.3 Random gradient-like expectation value minimization

The following code implements the random optimization method introduced in section 4.2.2. The maximum number of iterations is defined as `max_steps` and the number of significant digits required to converge is defined as `convergence_requirement`, values for `stuck_counter` and `convergence_counter` are chosen according to performance requirements.

```
def operator_o1(N,a):
  return (position(N)**2-a**2*qeye(N))**2

def operator_o2(N,a,z):
  plus = 1j*momentum(N)*a
  minus = -1j*momentum(N)*a
  return (-1/4)**z*(minus.expm()-plus.expm())**(2*z)

def dynamic_precision_random_optimisation(N, a, max_steps, initial_state,
  convergence_requirement):

  current_state = initial_state
  operator = operator_o1(N,a) + operator_o2(N,a,500)
  stuck_counter, convergence_counter, precision = (0, 0, 10)

  for step in range(max_steps):

    states = []
    qualities = []
    noise = rand_ket(N)

    if stuck_counter == 100:
      stuck_counter = 0
      precision *= 10

    for i in range(-1, 2):
      temp_state = (current_state+(i/precision)*noise).unit()
      states.append(temp_state)
      qualities.append(np.abs(expect(operator,temp_state)))
    best_quality = min(qualities)

    if np.round(best_quality, convergence_requirement)
    == np.round(qualities[1], convergence_requirement):
      convergence_counter += 1
    else:
      convergence_counter = 0

    if best_quality == qualities[1]:
      stuck_counter += 1

    else:
      current_state=states[qualities.index(best_quality)]
      stuck_counter = 0

    if convergence_counter == 1000:
      print(f"optimization converged in {step} steps")
      return current_state

  print("unsuccessful optimization, maximum steps reached")
  return current_state
```

A.4 Repeated random expectation value minimization

This is the code associated with fig. 4.4. A run of `repeated_random_quality_optimization` creates a `.csv` file which gets filled in with data, where each row corresponds to a quantum state, and where the first column is filled with values of $\left\langle \hat{O}(\alpha) \right\rangle$, the second column with $\sqrt{F_{\mathrm{QND}}}$ and the third column with $\sqrt{F_{\mathrm{BS}}}$. It also saves all the optimized states as `optimised_xx.qu`, where `xx` is the number of the optimization run. The `random_quality_optimization` function is based upon A.3 with some additional options available.

```
def repeated_random_quality_optimization(runs, N, a, max_steps, convergence_requirement, weight, initial_precision, stuck_limit, convergence_limit):

  meas_projector = ket2dm(find_optimal_p0(N))

  for run in range(runs):
    random_quality_optimization(N, a, max_steps, convergence_requirement, weight, initial_precision, stuck_limit, convergence_limit, meas_projector)

def random_quality_optimization(N, a, max_steps, convergence_requirement, weight, initial_precision, stuck_limit, convergence_limit, meas_projector):

  current_state = rand_ket(N)
  operator = operator_o1(N,a) + weight*operator_o2(N,a,500)
  stuck_counter, convergence_counter, precision = (0, 0, initial_precision)

  x0 = tensor(position(N), identity(N))
  p1 = tensor(identity(N), momentum(N))
  a0 = tensor(destroy(N), identity(N))
  a1 = tensor(identity(N), destroy(N))
  qnd_unitary = (-1j*p1*x0).expm()
  bs_unitary = (-(np.pi/4)*(a0.dag()*a1-a1.dag()*a0)).expm()
  mode1_in = basis(N,0)
  qnd_optimal_cond_out = ket2dm(displace(N, a/np.sqrt(2))*basis(N,0)+displace(N, -a/np.sqrt(2))*basis(N,0)).unit()
  bs_optimal_cond_out = ket2dm(displace(N,a/2)*squeeze(N,np.log(2)/2)*basis(N,0)+displace(N,-a/2)*squeeze(N,np.log(2)/2)*basis(N,0)).unit()

  with open(f"_randomoptimization_N{N}a{a}w{weight}.csv", "a", newline='') as csvfile:
    csv_writer = csv.writer(csvfile)

    for step in range(max_steps):

      states = []
      qualities = []
      noise = rand_ket(N)

      if stuck_counter == stuck_limit:
        stuck_counter = 0
        precision *= 5

      for i in range(-1, 2):
        temp_state = (current_state+(i/precision)*noise).unit()
        states.append(temp_state)
        qualities.append(np.abs(expect(operator,temp_state)))
      best_quality=min(qualities)

```

```
        if np.round(best_quality,convergence_requirement) == np.round(qualities[1],
    convergence_requirement):
          convergence_counter += 1
        else:
          convergence_counter = 0

        if best_quality == qualities[1]:
          stuck_counter += 1
        else:
          current_state=states[qualities.index(best_quality)]
          stuck_counter = 0

        mode0_in = current_state
        rho_in = ket2dm(tensor(mode0_in, mode1_in))

        qnd_out = qnd_unitary.dag()*rho_in*qnd_unitary
        qnd_cond_out = (((qnd_out*tensor(meas_projector,identity(N))).ptrace(1))).unit()
        bs_out = bs_unitary.dag()*rho_in*bs_unitary
        bs_cond_out = (((bs_out*tensor(meas_projector,identity(N))).ptrace(1))).unit()

        qnd_fid = fidelity(qnd_cond_out, qnd_optimal_cond_out)
        bs_fid = fidelity(bs_cond_out, bs_optimal_cond_out)

        csv_writer.writerow([best_quality, qnd_fid, bs_fid])

        if convergence_counter == convergence_limit:
          filename = "optimised_"
          suffix = 0

          while os.path.exists(filename + str(suffix) + ".qu"):
            suffix += 1

          filename += str(suffix)
          qsave(current_state, filename)

          print(f"the optimisation has converged after {step} steps at the value <O> = {np.
    round(best_quality, convergence_requirement)}\nthe generated state has been saved into {
    filename}.qu")

          return current_state

    print(f"the optimisation has not converged after {step} steps, lowest value <O> = {np.
    round(best_quality, convergence_requirement)}")

    return current_state
```